Spiny chondrichthyan from the lower Silurian of South China

Andreev, Plamen; Sansom, Ivan; Li, Qiang; Zhao, Wenjin; Wang, Jianhua; Wang, Chun-Chieh; Peng, Lijian; Jia, Liantao; Qiao, Tuo ; Zhu, Min

DOI:
10.1038/s41586-022-05233-8

Spiny chondrichthyan from the lower Silurian of South China

Plamen S. Andreev1,2†, Ivan J. Sansom3†, Qiang Li1,2†, Wenjin Zhao2,4,5, Jianhua Wang1, Chun-Chieh Wang6, Lijian Peng1, Liantao Jia2, Tuo Qiao2,4, Min Zhu2,4,5*

1Research Center of Natural History and Culture, Qujing Normal University, Qujing 655011, Yunnan Province, China. 2Key CAS Laboratory of Vertebrate Evolution and Human Origins, Institute of Vertebrate Paleontology and Paleoanthropology, Chinese Academy of Sciences (CAS), Beijing 100044, China. 3School of Geography, Earth and Environmental Sciences, University of Birmingham, UK. 4CAS Center for Excellence in Life and Paleoenvironment, Beijing 100044, China. 5University of Chinese Academy of Sciences, Beijing 100049, China. 6National Synchrotron Radiation Research Center, Hsinchu 30076, Taiwan.

*Corresponding author: zhumin@ivpp.ac.cn.

†These authors contributed equally to this work.

Summary paragraph

Modern representatives of chondrichthyans (cartilaginous fishes) and osteichthyans (bony fishes and tetrapods) exhibit contrasting skeletal anatomy and development[1-4] that underscore the distant evolutionary split[5-7] of the two clades. Recent work on upper Silurian and Devonian jawed vertebrates[7-10] has exposed similar skeletal conditions that blur conventional distinctions between osteichthyans, chondrichthyans and their jawed gnathostome ancestors. Here we describe the remains (dermal plates, scales and fin spines) of a chondrichthyan, *Fanjingshania renovata* gen. et sp. nov., from the lower Silurian of China that predates the earliest articulated fossils of jawed vertebrates[10-12]. *Fanjingshania* possesses dermal shoulder girdle plates and a complement of fin spines of striking anatomical similarity to those recorded in a subset of stem chondrichthyans[5,7,13] (climatiid 'acanthodians'[14]). Uniquely among chondrichthyans, however, it demonstrates osteichthyan-like resorptive shedding of scale odontodes and absence of odontogenic tissues in spines. Our results identify independent acquisition of these conditions in the chondrichthyan stem group, adding *Fanjingshania* to an increasing number of taxa[7,15] nested within traditionally-defined 'acanthodians'[16]. The discovery of *Fanjingshania* provides the strongest support yet for a proposed[7] early Silurian radiation of jawed vertebrates prior to their widespread appearance[5] in the fossil record in the Lower Devonian.

Hypotheses[17,18] of skeletal evolution within the principal divisions of early jawed vertebrates (osteichthyans, chondrichthyans and stem-gnathostome 'placoderms') have recently come under scrutiny following reports[8-10,19] of traditionally recognised crown-group conditions (e.g. endochondral bone, marginal jaw bones) in the stem lineage among 'placoderms' as well as 'placoderm'-like dermal scales in chondrichthyans[7]. In concert with these data from upper Silurian and Devonian specimens, phylogenies[5-7] of early jawed vertebrates expose gaps in the fossil record that extend back well into the Upper Ordovician and predict significant range extensions for a number of important lineages. Upper Ordovician (Sandbian) and lower Silurian (Llandovery) remains of isolated dermal scales and spines attributed to acanthodian-grade stem chondrichthyans[20,21] and enigmatic groups such mongolepids[22-24], sinacanthids[23,25] and elegestolepids[20,26] provide further evidence of early diversity. Nevertheless, due to the absence of articulated fossils and characters unequivocally linking them to established groups, the incorporation of these specimens into existing phylogenetic schemes of early vertebrates remains problematic[5,7].

Here we describe a c. 439-million-year-old chondrichthyan from the middle Llandovery of South China, whose remains were extracted from bone bed samples of the Rongxi Formation at Shiqian (Extended Data Fig. 1). The new taxon is based on abundant isolated remains and fragments of fused skeletal components and represents the stratigraphically oldest jawed vertebrate with a clearly established dermoskeletal anatomy. This discovery provides the first substantive morphological and developmental data from a chondrichthyan occurring c. 20 million years prior to the earliest chondrichthyan body fossils[5,7] and supports early estimates for the timing of the initial evolutionary radiation of jawed vertebrates.

Systematic palaeontology

Chondrichthyes Huxley, 1889

Fanjingshania renovata gen. et sp. nov.

Etymology. '*Fanjingshania'*, after Mount Fanjingshan, situated c. 100 km northeast of the type locality; '*renovata',* Latin for renewal (*renovatus*), alluding to the remodelling in the dermal skeleton of the species.

Holotype. Portion of a ventral (pinnal) shoulder girdle dermal plate fused to a fragment of a pectoral fin spine, IVPP (Institute of Vertebrate Paleontology and Paleoanthropology) V27433.1 (Figs. 1g, 2a–c and Extended Data Fig. 4c).

Referred material. Over 1000 isolated specimens including: head (tectal and postorbital) tesserae (Fig. 1s and Extended Data Fig. 2a, b), trunk scales, fused sclerotic plates (Fig. 1r), an incomplete branchiostegal plate (Fig. 1q), pectoral, prepelvic, pelvic, dorsal and anal fin spines (Fig. 1e, f, h–o, u–w and Extended Data Fig. 3), incomplete lorical (median) and pinnal (paired) shoulder girdle plates fused to complete or partial spines (Fig. 1a–d, g, p, t and Extended Data Fig. 4).

Locality and horizon. Shiqian-Tunping section at Leijiatun village (Shiqian County), Guizhou Province, China (Extended Data Fig. 1). Rongxi Formation, *Ozarkodina guizhouensis* conodont biozone (c. 439 Ma; late Aeronian, Llandovery, Silurian).

Diagnosis (as for genus). Jawed vertebrate with paired (pinnal) dermal shoulder girdle plates, each fused to a pair of prepectoral spines, a pectoral and a prepelvic (admedian) fin spine; ventral and ascending laminae of the pinnal plates extended to the posterior edge of pectoral fin spines; median (lorical) shoulder girdle plate with a

low conical spine; fin spines are laterally compressed and broad-based and carry ornamenting ridges studded with fine tubercles; trunk scale crowns possess a linear array of primary odontodes sculpted by discontinuous nodose ridges; the anterior of trunk scale crows features a conspicuous pustule or a large, dome-shaped replacement odontode; dentine developed only in scale/tessera crowns.

Remarks. Attribution of dermoskeletal elements to *Fanjingshania* is based on their tissue composition (cellular bone and/or atubular dentine), surface sculpture (nodose ridges and fine tuberculate ornament), developmental features (hard-tissue resorption and scale crown growth), as well as direct evidence from fused elements. In turn, the assignment of fin spines, dermal plates and tesserae to specific body positions (Fig. 2x, y and Extended Data Fig. 7) rests on similarities with the dermoskeletal anatomy of climatiids[13,14,27,28], particularly that of *Climatius reticulatus*[27,28].

Isolated tooth whorls were also recovered from our Rongxi samples from Shiqian (Extended Data Fig. 1). The disarticulated nature and the yet uncertain tissue composition of the tooth whorls result in the absence of direct morphological and histological evidence that could support their attribution to *Fanjingshania*. This is further complicated by the co-occurrence of whorls with the fragmentary remains of other, still to be described, chondrichthyans that are recognised on the basis of distinct fin spines and scales. We therefore formally described the tooth whorl material elsewhere, following established practice[29] to erect a new taxon for disarticulated vertebrate remains that can be distinguished by a unique set of features.

Elements of the dermal skeleton

The holotype of *Fanjingshania* (Figs. 1g, 2a–c) and other figured material (Figs. 1t, 2j and Extended Data Figs. 4a, b, d, 5d, e) represent articulated dermal scales fused together by a basal plate that are fused to a fragment of a spine wall. The latter is either level with the basal plate or makes contacts with it at an angle. These specimens are recognised as remnants of pectoral fin spines fused to paired ventral plates of the shoulder girdle (pinnal plates) of a compound type documented in a number of stem chondrichthyans (e.g. *Ptomacanthus*[30], *Sabrinacanthus*[28] and *Diplacanthus*[31]). Within total-group Chondrichthyes the pectoral girdle is the only site where large (macromeric) dermal ossifications are associated with spines[32]. 'Placoderm' or osteichthyan origin of these elements is considered unlikely as there are no known examples of pinnal-like multi-component dermal plates in either of the two groups[33-35].

The scales carried by the pinnal plates vary in size (Fig. 2a) and have irregular rhomboid to oblong crowns ornamented with nodose ridges adorned by fine tubercles. The pectoral fin spine fragments of V27433.1–V27433.7 preserve up to 13 flat-topped nodose ridges studded with tubercles. The spine ridges are of variable width and can bifurcate as well as assume a 'string of pearls' appearance near the junction with the plate (Fig. 1t).

Other partial plates (Figs. 1c, d, 2d, e) with the basal plate/dermal scale structure of the pinnal elements fuse around the periphery of a low, broad-based spine with recurved, posteriorly offset apex. The spines are longer than high and possess up to 11 nodose ridges per lateral side that become discontinuous basally. These features are also seen in climatiid 'acanthodians' (e.g. *Erriwacanthus*[28,36], *Sabrinacanthus*[28] *and Climatius*[27]) and where there is a fusion of the posterior

margin of the pinnal plates with a pair of prepelvic (admedian) fin spines formed medially of the pectoral fin spines.

Two fragmentary specimens (Fig. 1a, b and Extended Data Fig. 4j–l) possess laterally compressed pairs of fused spines of unequal size. The spines are nearly symmetrical, ornamented with rows of tubercules that extend on to incompletely preserved dermal plates that are continuous with the spine margins. In both specimens, one of the lateral plate laminae is angled and tapers towards as well as extends beyond the smaller of the spine pair (Fig. 1a). These elements morphologically correspond to the prepectoral spines integrated into the anterior pinnal plates of stem chondrichthyans (e.g. in *Parexus*, *Climatius*, *Ptomacanthus, Brachyacanthus* and *Euthacanthus*)[14,27,28,30], with the dermal shelves of V27436.1, 2 representing the remnants of ascending and ventral pinnal laminae (Fig. 1a, b and Extended Data Fig. 4j, l).

A partial plate (V27441.1, Fig. 1p) is distinguished from other *Fanjingshania* material by a low conical spine aligned to a prominent bulge of the plate margin. The spine is flanked by two basal plate-supported scales of the type observed in the pinnal elements of *Fanjingshania*. The distinct plate margins and spine of V27441.1 are features of the median ventral (lorical) plates of *Climatius*[27,28] and *Parexus*[14] and identify the specimen as such.

Incomplete isolated fin spines (Fig. 1e, f, h–o, u–w and Extended Data Fig. 3) attributed to *Fanjingshania* possess the nodose ridge sculpture seen in the fin spine fragments fused to plates of the dermal pectoral girdle (Fig. 1t). Their assignment to specific positions in the body (Fig. 1x, y) is dictated by close morphological similarity to the fin spine types of *Climatius reticulatus*[27,28]. Pectoral fin spines (Fig. 1e, f)

159 exhibit strong lateral compression and broad, recured profiles. Their anterior edge is
160 shaped into a well-developed rib, whereas the posterior one bears a deep sulcus.
161 Spines recognised as anterior dorsal (Fig. 1n, o) resemble in overall appearance the
162 pectoral fin spines but are distinguished by a more upright apex. More acuminate
163 and less recurved spine types are identified as posterior dorsal (Fig. 1l, m), pelvic
164 (Fig. 1h, i) and anal (Fig. 1j, k) fin spines. Other spine material assigned to
165 *Fanjingshania* comprises low, laterally flattened spines with an acutely sloped,
166 uneven anterior edge and a second incipient apex in a posterior position (Fig. 1u–w).
167 Differences in size and angle of curvature between these allow to differentiate three
168 morphologies representing paired ventral (prepelvic) spines of the type developed
169 posterior of the pectoral girdle in a range of stem chondrichthyans (e.g. in
170 diplacanthids[31] and climatiids[14,27,28]).

171 Isolated trunk scales belonging to *Fanjingshania* have deltoid to ovoid crowns
172 with symmetric and asymmetric outlines (Fig. 2f, h and Extended Data Fig. 2c–k).
173 Crown surfaces reveal the margins of apposed odontodes (Fig. 2f, h) of increasing
174 size ornamented in non-abraded specimens by tuberculated ridges. The scale
175 crowns extend posteriorly over rhombic bases with substantially smaller footprints
176 and a prominent neck-like constriction. In some specimens the anterior odontodes
177 are truncated or fully excavated and replaced by a large acuminate odontode raised
178 above the crown surface (Fig. 2f, g).

179 Dermoskeletal growth and tissue structure

180 Pinnal plate scales and isolated trunk scales possess a row of appositionally
181 arranged crown odontodes as well as an anterior cluster of secondary odontodes
182 (Fig. 2b, h). Atubular dentine with incremental depositional lines and dispersed

183 mineralised spherites is seen in thin sections as the sole component of the
184 odontodes (Fig. 2g, i and Extended Data Figs. 2p, q, 5e). The crowns are supported
185 by bases of lamellar bone harbouring densely packed cell lacunae and pervaded by
186 apically converging fibre spaces (Fig. 2g, i).

187 The pinnal plates share the cellular bone composition of the bases of the
188 scales to which they are fused (Fig. 2c, e, j). The plates' cellular bone is continuous
189 with the walls of pectoral and admedian spines (Fig. 2c, j and Extended Data Fig. 4a,
190 h) that consist entirely of this tissue, including an outer vascular zone and the
191 ornamenting ridges (Fig. 1c, d and Extended Data Fig. 4a, d). Cellular bone
192 composition is also recognised in isolated fin spines (Extended Data Fig. 3v, w),
193 where globular calcified cartilage is present apically inside the spines' central cavity.

194 Scale resorption is evidenced in the pinnal plate material by longitudinally truncated
195 crowns at different states of completeness (Fig. 1a, d and Extended Data Fig. 5f–i).
196 Resorption surfaces are also observed in isolated trunk scales (Fig. 1i and Extended
197 Data Fig. 5a, c, e) but form only anteriorly where a deep cavity marks the partial
198 removal or shedding of odontodes and the apical portion of the base. The resorption
199 cavity is covered by a large acuminate replacement odontode (Fig. 2g and Extended
200 Data Fig. 5a, c) at a later stage of scale development.

201 *Fanjingshania* is an outlier among early vertebrates in presenting a unique
202 mix of jawed vertebrate plesiomorphies and apomorphies pertaining to
203 dermoskeletal development (Fig. 3). Of these, only the formation of a single row of
204 consecutive scale-odontode generations has been recognised in stem
205 chondrichthyans described from articulated material (in *Parexus*[14], *Brochoadmones*[37], *Seretolepis*[38] and *Kathemacanthus*[38]). The atubular dentine of

Fanjingshania conforms to the characteristics of a tissue type known as lamellin[22,24], with distribution previously restricted to enigmatic scale- and spine-based chondrichthyans (mongolepids[22-24,39] and sinacanthids[23,24,40]) the majority of which occur in the Telychian (lower Silurian). Intriguingly, other chondrichthyan-like remains recovered from mongolepid/sinacanthid assemblages, such as the scale-based *Yuanolepis bachunensis*[23] and spine morphology A[24], share scale and spine structure and histology with *Fanjingshania*.

The dermoskeletal remodelling in *Fanjingshania* has not previously been recognised within the total-group Chondrichthyes[1,17]. In trunk scales this is evident by the shedding of odontodes through resorptive removal of dentine and dermal bone and the deposition of new odontode generations on the exterior surface (Fig. 1f, g and Extended Data Fig. 5a, c, e) The closest examples of this replacement mechanism are identified in the oral and extra-oral dermal skeleton of some stem and crown osteichthyans[41-45]. Odontode resorption in *Fanjingshania*, however, is not site specific as in osteichthyans but instead proceeds areally by episodic removal of multiple odontode generations. Its odontode replacement pattern also deviates from that of other vertebrates[3] by reducing the number of scale odontodes as shedding proceeds.

Phylogenetic results

On the basis of limited character data determined by the fragmentary nature of the material, *Fanjingshania* was resolved under parsimony and Bayesian optimality criteria (Fig. 3 and Extended Data Fig. 6) as a derived stem chondrichthyan nested within climatiid 'acanthodians'[14,30]. A consequence of this placement is a c. 20 million year age increase to internal nodes of the chondrichthyan stem relative to recent

231 estimates[5,7]. These results pull back the earliest occurrence date for climatiids to the
232 early Silurian and similarly extend the ghost ranges of other conventional
233 'acanthodian' groupings[14,31,38,46,47] away from their first documented appearances in
234 the late Silurian–Early Devonian (Fig.3). A corresponding extension of the
235 osteichthyan stem deep into the Silurian is also predicted by our analysis (Fig. 3),
236 which is in accordance with morphological clock estimates[6] for the divergence of
237 osteichthyans and chondrichthyans. The absence of recognisable osteichthyan
238 remains from samples coeval with *Fanjingshania* might be explained by preservation
239 bias against isolated teeth and body-fossils in strata of comparable age.

240 *Fanjingshania,* and potentially lamellin-forming chondrichthyans at large
241 (including mongolepids[22-24] and sinacanthids[23,25,40]), provide evidence for the
242 existence of taxa with a climatiid-type dermoskeletal anatomy in the lower Silurian.
243 This infers a protracted diversification model for the climatiids as well as for the
244 remainder of the 'acanthodian' lineages, for which direct fossil evidence from the
245 Upper Ordovician–lower Silurian is still missing[39,48,49]. A possible factor contributing
246 to this discrepancy, akin to the barren osteichthyan record, could be the under-
247 sampling of pre-Devonian vertebrate assemblages.

248 *Fanjingshania* adds a number of jawed vertebrate homoplasies (e.g.
249 resorptive odontode shedding and absence of odontogenic tissues in dermal spines)
250 to the chondrichthyan stem within a phylospace occupied by traditionally defined
251 'acanthodians'[16]. These results are in conflict with the current view[3] of total-group
252 Chondrichthyes as primitively lacking competence to grow dermoskeletal tissues
253 through resorption and remodelling. They increase the disparity of character
254 combinations in early chondrichthyans and provide much needed data on the

sequence of evolutionary changes leading up to the emergence of crown chondrichthyans.

Online content

Any methods, additional references, Nature Research reporting summaries, source data, extended data, supplementary information, acknowledgements, peer review information; details of author contributions and competing interests; and statements of data and code availability are available at https://doi.org/XXXXX

1 Dean, M. N., Mull, C. G., Gorb, S. N. & Summers, A. P. Ontogeny of the tessellated skeleton: insight from the skeletal growth of the round stingray *Urobatis halleri*. *J. Anat.* **215**, 227-239 (2009).

2 Seidel, R., Blumer, M., Chaumel, J., Amini, S. & Dean, M. N. Endoskeletal mineralization in chimaera and a comparative guide to tessellated cartilage in chondrichthyan fishes (sharks, rays and chimaera). *J. Royal Soc. Interface* **17**, 20200474 (2020).

3 Sire, J. Y., Donoghue, P. C. & Vickaryous, M. K. Origin and evolution of the integumentary skeleton in non-tetrapod vertebrates. *J. Anat.* **214**, 409-440 (2009).

4 Witten, P. E. & Huysseune, A. A comparative view on mechanisms and functions of skeletal remodelling in teleost fish, with special emphasis on osteoclasts and their function. *Biol. Rev.* **84**, 315-346 (2009).

5 Brazeau, M. D. & Friedman, M. The origin and early phylogenetic history of jawed vertebrates. *Nature* **520**, 490-497 (2015).

6 King, B., Qiao, T., Lee, M. S., Zhu, M. & Long, J. A. Bayesian morphological clock methods resurrect placoderm monophyly and reveal rapid early evolution in jawed vertebrates. *Syst. Biol.* **66**, 499-516 (2017).

7 Coates, M. I. *et al.* An early chondrichthyan and the evolutionary assembly of a shark body plan. *Proc. R. Soc B* **285**, 20172418 (2018).

8 Brazeau, M. *et al.* Endochondral bone in an Early Devonian 'placoderm' from Mongolia. *Nat. Ecol. Evol.* **4**, 1477-1484 (2020).

9 Giles, S., Friedman, M. & Brazeau, M. D. Osteichthyan-like cranial conditions in an Early Devonian stem gnathostome. *Nature* **520**, 82-85 (2015).

10 Zhu, M. *et al.* A Silurian maxillate placoderm illuminates jaw evolution. *Science* **354**, 334-336 (2016).

11 Burrow, C. J. & Rudkin, D. Oldest near-complete acanthodian: the first vertebrate from the Silurian Bertie Formation Konservat-Lagerstätte, Ontario. *PLoS One* **9**, e104171 (2014).

12 Zhu, M. *et al.* The oldest articulated osteichthyan reveals mosaic gnathostome characters. *Nature* **458**, 469-474 (2009).

13 Dearden, R. P. *et al.* A revision of *Vernicomacanthus* Miles with comments on the characters of stem-group chondrichthyans. *Pap. Palaeontol.* **7**, 1949-1976 (2021).

14 Burrow, C. J., Newman, M. J., Davidson, R. G. & den Blaauwen, J. L. Redescription of *Parexus recurvus*, an Early Devonian acanthodian from the Midland Valley of Scotland. *Alcheringa* **37**, 392-414 (2013).
15 Maisey, J. *et al.* in *Evolution and Development of Fishes* (eds Johanson, Z., Underwood, C. & Richter, M.) 87-109 (Cambridge Univ. Press, 2019).
16 Denison, R. *Acanthodii*. Vol. 5 (Gustav Fischer Verlag, 1979).
17 Donoghue, P. C. J., Sansom, I. J. & Downs, J. P. Early evolution of vertebrate skeletal tissues and cellular interactions, and the canalization of skeletal development. *J. Exp. Zool. Part B: Mol. Dev. Evol.* **306**, 278-294 (2006).
18 Giles, S., Rücklin, M. & Donoghue, P. C. Histology of "placoderm" dermal skeletons: Implications for the nature of the ancestral gnathostome. *J. Morphol.* **274**, 627-644 (2013).
19 Zhu, M. *et al.* A Silurian placoderm with osteichthyan-like marginal jaw bones. *Nature* **502**, 188-193 (2013).
20 Karatajūtė-Talimaa, V. & Predtechenskyj, N. The distribution of the vertebrates in the Late Ordovician and Early Silurian palaeobasins of the Siberian Platform. *Bull. Mus. natl. Hist. nat. 4è. sér. C* **17**, 39-55 (1995).
21 Karatajūtė-Talimaa, V. & Smith, M. M. Early acanthodians from the Lower Silurian of Asia. *Earth Environ. Sci. Trans. R. Soc. Edinb.* **93**, 277-299 (2002).
22 Andreev, P. S. *et al.* The systematics of the Mongolepidida (Chondrichthyes) and the Ordovician origins of the clade. *PeerJ* **4**, e1850 (2016).
23 Andreev, P. S. *et al.* Early Silurian chondrichthyans from the Tarim Basin (Xinjiang, China). *PLoS One* **15**, e0228589 (2020).
24 Sansom, I. J., Aldridge, R. & Smith, M. M. A microvertebrate fauna from the Llandovery of South China. *Earth Environ. Sci. Trans. R. Soc. Edinb.* **90**, 255-272 (2000).
25 Zhu, M. Early Silurian sinacanths (Chondrichthyes) from China. *Palaeontology* **41**, 157-171 (1998).
26 Andreev, P. S. *et al. Elegestolepis* and its kin, the earliest monodontode chondrichthyans. *J. Vertebr. Paleont.* **37**, e1245664 (2016).
27 Burrow, C. J., Davidson, R. G., Den Blaauwen, J. L. & Newman, M. J. Revision of *Climatius reticulatus* Agassiz, 1844 (Acanthodii, Climatiidae), from the Lower Devonian of Scotland, based on new histological and morphological data. *J. Vertebr. Paleont.* **35**, e913421 (2015).
28 Miles, R. S. Articulated acanthodian fishes from the Old Red Sandstone of England: with a review of the structure and evolution of the acanthodian shoulder-girdle. *Bull. Br. Mus. Nat. Hist. Geol.* **24**, 111-213 (1973).
29 Ginter, M., Hampe, O., Duffin, C. J. & Schultze, H. *Chondrichthyes. Paleozoic Elasmobranchii: Teeth.* Vol. 3D (Verlag Dr Friedrich Pfeil, 2010).
30 Dearden, R. P., Stockey, C. & Brazeau, M. D. The pharynx of the stem-chondrichthyan *Ptomacanthus* and the early evolution of the gnathostome gill skeleton. *Nat. Commun.* **10**, 2050 (2019).
31 Burrow, C., den Blaauwen, J., Newman, M. & Davidson, R. The diplacanthid fishes (Acanthodii, Diplacanthiformes, Diplacanthidae) from the Middle Devonian of Scotland. *Palaeontol. Electron.* **19**, 1-83 (2016).
32 Maisey, J. G. *et al.* Pectoral morphology in *Doliodus*: bridging the 'acanthodian'-chondrichthyan divide. *Am. Mus. Novit.* **2017**, 1-15 (2017).
33 Denison, R. H. *Placodermi*. Vol. 2 (Gustav Fischer Verlag, 1978).
34 Long, J. A. *et al.* Copulation in antiarch placoderms and the origin of gnathostome internal fertilization. *Nature* **517**, 196-199 (2015).
35 Zhu, M. *et al.* Fossil fishes from China provide first evidence of dermal pelvic girdles in osteichthyans. *PLoS One* **7**, e35103 (2012).
36 Ørvig, T. Some new acanthodian material from the Lower Devonian of Europe. *Zool. J. Linn. Soc.* **47**, 131-153 (1967).

37 Hanke, G. F. & Wilson, M. V. Anatomy of the Early Devonian acanthodian *Brochoadmones milesi* based on nearly complete body fossils, with comments on the evolution and development of paired fins. *J. Vertebr. Paleont.* **26**, 526-537 (2006).
38 Hanke, G. & Wilson, M. in *Morphology, Phylogeny and Paleobiogeography of Fossil Fishes* (eds Elliott, D. K., Maisey, J. G., Yu, X. & Miao, D.) 159-182 (Verlag Dr. Friedrich Pfeil, 2010).
39 Sansom, I. J. & Andreev, P. S. in *Evolution and Development of Fishes* (eds Johanson, Z., Underwood, C. & Richter, M.) 59-70 (Cambridge Univ. Press, 2019).
40 Sansom, I. J., Wang, N.-Z. & Smith, M. The histology and affinities of sinacanthid fishes: primitive gnathostomes from the Silurian of China. *Zool. J. Linn. Soc.* **144**, 379-386 (2005).
41 Chen, D., Blom, H., Sanchez, S., Tafforeau, P. & Ahlberg, P. E. The stem osteichthyan *Andreolepis* and the origin of tooth replacement. *Nature* **539**, 237-241 (2016).
42 Sire, J. Y., Marin, S. & Allizard, F. Comparison of teeth and dermal denticles (odontodes) in the teleost Denticeps clupeoides (Clupeomorpha). *J. Morphol.* **237**, 237-255 (1998).
43 Doeland, M., Couzens, A. M., Donoghue, P. C. & Rücklin, M. Tooth replacement in early sarcopterygians. *R. Soc. Open Sci.* **6**, 191173 (2019).
44 Chen, D. *et al.* The developmental relationship between teeth and dermal odontodes in the most primitive bony fish *Lophosteus*. *eLife* **9**, e60985 (2020).
45 Chen, D. *et al.* Development of cyclic shedding teeth from semi-shedding teeth: the inner dental arcade of the stem osteichthyan *Lophosteus*. *R. Soc. Open Sci.* **4**, 161084 (2017).
46 Burrow, C. J., Newman, M., Den Blaauwen, J., Jones, R. & Davidson, R. The Early Devonian ischnacanthiform acanthodian *Ischnacanthus gracilis* (Egerton, 1861) from the Midland Valley of Scotland. *Acta Geol. Pol.* **68**, 335–362 (2018).
47 Turner, S., Burrow, C. J. & Warren, A. *Gyracanthides hawkinsi* sp. nov.(Acanthodii, Gyracanthidae) from the Lower Carboniferous of Queensland, Australia, with a review of gyracanthid taxa. *Palaeontology* **48**, 963-1006 (2005).
48 Zhao, W.-J. & Zhu, M. Siluro-Devonian vertebrate biostratigraphy and biogeography of China. *Palaeoworld* **19**, 4-26 (2010).
49 Žigaitė, Ž., Karatajūtė-Talimaa, V. & Blieck, A. Vertebrate microremains from the Lower Silurian of Siberia and Central Asia: palaeobiodiversity and palaeobiogeography. *J. Micropalaeont.* **30**, 97-106 (2011).

Methods

The fossil material assigned to *Fanjingshania* consists of over 1000 isolated fin spines, spines, tesserae, scales and plates (Table S1). The specimens were recovered from residues of sediment samples (35SQTP) disaggregated with buffered 8% acetic acid. The 35SQTP samples were collected from the upper beds of the Rongxi Formation exposed in the Shiqian-Tunping section (Extended Data Fig. 1) near the village of Leijiatun, Shiqian County, Guizhou Province, China[50]. All

studied specimens were reposited at the Institute of Vertebrate Paleontology and Paleoanthropology (IVPP), Chinese Academy of Sciences, Beijing.

X-ray tomography

Synchrotron X-ray tomography was used to image seven specimens (V26641, V27433.1, V27434.1, 3, V27435.1, 13, 14, 26 and V27437.15) at beamlines BL01A1 and BL01B1 of the Taiwan Light Source (TLS), National Synchrotron Radiation Research Center (NSRRC), Taiwan. Radiograph data were acquired with a parallel semi-white-light hard X-ray beam at ≥ 4 keV over a 180° rotation arc at 0.3° increments. The resultant datasets contain 601 radiographs of 1600 X 1200-pixel size and 2.76 μm per pixel resolution. Radiograph alignment was enhanced in Matlab R2014b by processing the data with the fast projection matching (Faproma) algorithm developed by Wang[51]. Reconstructions of tomographic slices from radiograph projections was performed in VGSTUDIO MAX 3.0 and produced sets of 1200 slices per specimen.

Over 600 specimens, including illustrated material (V27435.7, V27437.4, 8–14, V27439.1, V27438.4, V27440.2, V27441.1, 2, 4–6, V27443.1), were examined at the Institute of Vertebrate Paleontology and Paleoanthropology (IVPP), Chinese Academy of Sciences with the X-ray micro-computed tomography scanner (225-3D-μCT) designed by the Institute of High Energy Physics, Chinese Academy of Sciences[52]. Another 6 scales, a pair of prepectoral spines and a fin spine fragment (V27435.15–20, V27436.1, V27437.16) were imaged with a Zeiss Xradia Versa 520 micro-CT scanner at the Yunnan Key Laboratory for Palaeobiology, Yunnan University, China and six scales (V27435.2, 21, 23–26) were imaged with a

Skyscan1172 micro-CT scanner at the School of Dentistry, University of Birmingham. The IVPP analyses produced radiograph datasets acquired over 360° rotation cycles that were converted in VGSTUDIO MAX 3.0 to 1748 x 556-pixel tomograms with a 5.33 µm per pixel resolution. The Zeiss Xradia Versa 520 radiograph data were generated over a 360° rotation arc at 50 keV and reconstructed in VGSTUDIO MAX 3.0 to produce 984 X 1009 pixel tomograms with pixel size of 3.63 µm. Radiographs from the Skyscan1172 analysis were acquired at 70 keV with the use of X-ray attenuating 0.5 mm Al filter and rotation set to 180°. Resultant tomograms are 1332 x 2000 pixels with resolution of 2.06 µm per pixel.

Volumetric reconstructions of specimens from tomographic slices was performed in Mimics 19.0.

Scanning electron microscopy

Surface features of 4 partial and complete fin spines, 29 scales, 5 pectoral plate fragments and a tectal tessera, including the illustrated V27433.5, V27435.6, 9, 11, 12, 27, V27441.3 and V27442.1, were documented uncoated with a Phenom ProX Desktop SEM at 5 keV at the School of Geography, Earth and Environmental Sciences, University of Birmingham.

Light microscopy

A pair of prepectoral spines (V27436.2), an admedian fin spine fused to a pinnal plate (V27434.2) and four fin spines (V27437.3, 5–7) were imaged with a GXM

XTL3101 stereo microscope at the School of Geography, Earth and Environmental Sciences, University of Birmingham.

A total of 40 specimens (tesserae, incomplete pinnal plates fused to pectoral fin spine fragments and partial and complete fin spines) were thin sectioned at Qujing Normal University, China. Nomarski DIC polarized light micrographs of the sections (including figured material V27433.2, 3, 6, V27434.4, V27435.4, 5, 8, 10, V27437.1, 2, 14, V27438.5) were imaged with an Olympus D12 digital camera mounted on an Olympus BX51 Fluorescent Microscope.

Phylogenetic analyses

We performed phylogenetic analyses under parsimony and Bayesian optimality criteria using a data matrix of 105 taxa and 292 characters (see Supplementary Data 7, 8). The matrix was compiled from characters and character codings from Brazeau et al.[8], Coates et al.[7], Dearden[53], Dearden et al.[30], Qiao[54] and Vaškaninová et al.[55] (see also List of characters and Supplementary Data).

The parsimony analysis was conducted in TNT version 1.5[56] under parsimony criteria by running a traditional search with TBR swapping algorithm set to save 100 trees per replication and limited to 1000 addition-sequence replicates. Trees were rooted by designating Galeaspida as an outgroup and a maximum of 100000 trees was kept in the memory. The analysis returned 5639 most parsimonious trees (920 steps each) from which we calculated 50 percent majority-rule consensus (926 steps) and strict consensus (1099 steps) trees (Supplementary Data 7). All characters were unordered and of equal weights with character states at internal nodes reconstructed as MPR sets in PAUP version 4.0a (build 169)[57].

Bootstrap values for the 50 percent majority-rule and strict consensus trees were calculated in TNT by resampling the data matrix over 100 bootstrap replicates using the traditional search option (Supplementary Data 7). The 50 percent majority-rule consensus tree (Fig. 3 and Extended Data Fig. 6a) and its branch length values was imported into R (version 4.0.2) and time adjusted with the R package paleotree 3.3.25[58]. The analysis was performed using the timePaleoPhy function of paleotree with mbl-type time scaling and pre-assigned taxon and tree root ages taken from King et al.[6] and other studies (Table S2).

A Bayesian analysis was conducted in MrBayes version 3.2.7a[59] using a MCMC statistical model, gamma-distribution rates and variable character-coding bias. The analysis was run for 10 million generations with a tree sampling frequency of 1000. Burn-in for tree samples was set at 25% and tree topology was constrained by designating Galeaspida as an outgroup and jawed gnathostomes as monophyletic (Supplementary Data 8).

Note on Figure 3

The line drawings and interpretation of dermoskeletal features of early jawed gnathostomes depicted in Fig. 3 based on data from: Béchard et al.[60] (*Bothriolepis*), Pearson and Westoll[61] (*Cheirolepis*), Miles[28] and Burrow et al.[5] (*Climatius*), Zhu et al.[19] (*Entelognathus*), Zhu et al.[35] (*Guiyu*), Hanke and Wilson[38] (*Kathemacanthus*) and Dupret[62] (*Kujdanowiaspis*).

Data availability

Investigated *Fanjingshania* specimens were assigned accession numbers (IVPP V27433–V27443) and deposited at the Institute of Vertebrate Paleontology and Paleoanthropology, Chinese Academy of Sciences, Beijing. Supplementary information nex, zip and ply format files are currently available at https://www.dropbox.com/sh/or0zqqt4seheael/AADZmI2kNWcJ77WI0a5zXePOa?dl=0 and will be published online in a publicly accessible repository (ADMorph) upon acceptance of the manuscript.

50 Wang, C.-Y. & Aldridge, R. J. Silurian conodonts from the Yangtze Platform, south China. *Spec. Pap. Palaeontol.* **83**, 1-135 (2010).

51 Wang, C.-C. Joint iterative fast projection Matching for fully Automatic Marker-free Alignment of nano-tomography Reconstructions. *Sci. Rep.* **10**, 7330 (2020).

52 Wang, Y. *et al.* Development and applications of paleontological computed tomography. *Vertebr. PalAsiat.* **57**, 84-92 (2019).

53 Dearden, R. P. *The anatomy and evolution of "acanthodian" stem-chondrichthyans* (Imperial College London, (2018).

54 Qiao, T., King, B., Long, J. A., Ahlberg, P. E. & Zhu, M. Early gnathostome phylogeny revisited: multiple method consensus. *PLoS One* **11**, e0163157 (2016).

55 Vaškaninová, V. *et al.* Marginal dentition and multiple dermal jawbones as the ancestral condition of jawed vertebrates. *Science* **369**, 211-216 (2020).

56 Goloboff, P. A. & Catalano, S. A. TNT version 1.5, including a full implementation of phylogenetic morphometrics. *Cladistics* **32**, 221-238 (2016).

57 Swofford, D. L. *PAUP*: Phylogenetic Analysis Using Parsimony* and other methods*. Version 4.0b10 (Sinauer Associates, 2002).

58 Bapst, D. W. paleotree: an R package for paleontological and phylogenetic analyses of evolution. *Methods Ecol. Evol.* **3**, 803-807 (2012).

59 Ronquist, F. & Huelsenbeck, J. P. MrBayes 3: Bayesian phylogenetic inference under mixed models. *Bioinformatics* **19**, 1572-1574 (2003).

60 Béchard, I., Arsenault, F., Cloutier, R. & Kerr, J. The Devonian placoderm fish Bothriolepis canadensis revisited with three-dimensional digital imagery. *Palaeontol. Electron.* **17**, 1-19 (2014).

61 Pearson, D. M. & Westoll, T. S. The Devonian actinopterygian Cheirolepis Agassiz. *Earth Environ. Sci. Trans. R. Soc. Edinb.* **70**, 337-399 (1979).

62 Dupret, V. Revision of the genus *Kujdanowiaspis* Stensiö, 1942 (Placodermi, Arthrodira,“Actinolepida”) from the Lower Devonian of Podolia (Ukraine). *Geodiversitas* **32**, 5-63 (2010).

Acknowledgements We thank Y.-M. Hou for the acquisition of the micro-CT X-ray data, Y. Hwu (Academia Sinica) and Y.-T. Weng (NSRRC) for performing and

assisting with the synchtrotron X-ray analyses, and Y.Z. Hu for her comments and advice during the volumetric reconstructions of the specimens. This research was supported by the Strategic Priority Research Program of the Chinese Academy of Sciences (XDA19050102, XDB26000000), the National Natural Science Foundation of China (41530102), the Key Research Program of Frontier Sciences, CAS (QYZDJ-SSW-DQC002), an Open Project Grant of the Key Laboratory of Vertebrate Evolution and Human Origins, IVPP, CAS (LVEHO19001), MOST 108-2116-M-213-001 (Taiwan), Chinese Postdoctoral Science Foundation grant (2019M663440) and the National Synchrotron Radiation Research Center, Taiwan (beamtime Projects No 2019-3-083-1 and 2019-3-185-1).

Author contributions Research design: M.Z., P.S.A., and I.J.S.; Fieldwork and sample collection: M.Z., W.Z, Q.L., J.W., L.J., T.Q., and L.P.; Data processing: Q.L., P.S.A., L.P., J.W., and M.Z.; Synchrotron X-ray tomography analyses: P.S.A., and C.W.; Manuscript text and figure preparation: P.S.A., I.J.S., Q.L., J.W., and M.Z.

Competing interests The authors declare no competing interests.

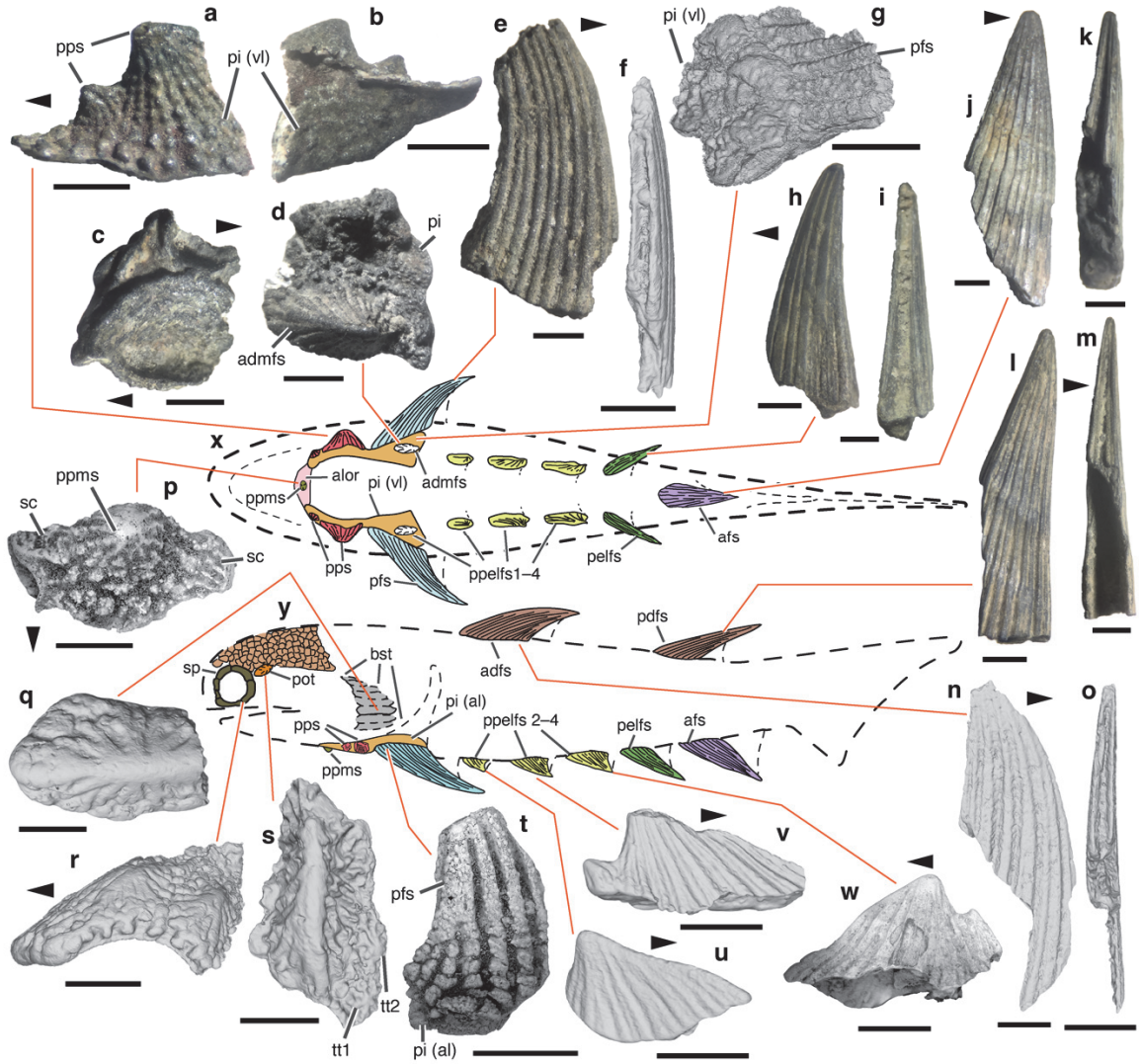

Fig. 1 | Dermoskeletal elements of *Fanjingshania renovata*. Volume renderings based on synchrotron (g) and microcomputed X-ray tomography data (f, n, o, q–s, u, v), scanning electron micrographs (p, t, w) and optical micrographs (a–e, h–m). Incomplete pinnal plate carrying two prepectoral spines (V27436.2) in **a**, external and **b**, visceral views. Incomplete pinnal plate fused to an admedian spine (V27434.2) in **c,** visceral and **d**, ventral views. **e**, Partial pectoral fin spine (V27437.3) in lateral view. **f**, Incomplete pectoral spine (V27437.4) in posterior view. **g**, Ventral oblique view of a pectoral fin spine fragment fused to a partial ventral lamina of a pinnal plate (V27433.1, holotype). **h**, Lateral and **i**, posterior views of an incomplete pelvic fin spine (V27437.7). Incomplete anal fin spine (V27437.6) in **j**, lateral and **k**, posterior views. Incomplete posterior dorsal fin spine (V27437.5) in **l**, lateral and **m**, posterior views. **n**, Lateral and **o**, posterior views of an incomplete anterior dorsal fin spine (V27437.8). **p**, Incomplete anterior lorical plate (V27442.1) in ventral view. **q**, Partial branchiostegal plate (V27439.1) in visceral view. **r**, Incomplete fused sclerotic plates (V27443.1) in lateral view. **s**, Postorbital tessera (V27440.2) in crown view. **t**, Pectoral plate fragment fused to a partial pinnal plate (V27433.4) in external view. (**u**–**w**), Lateral views of prepelvic fin spines (V27441.1–3) of increasingly more posterior positions. Schematic reconstruction of the dermal skeleton of *Fanjingshania renovata* in **x**, ventral and **y**, lateral views based on similarities of the material assigned to the new taxon (see also Supplementary Information) with the anatomy of climatiid stem chondrichthyans[14,27]. Line art adapted from Denison 1979[16]. Arrowheads point to anterior. adfs, anterior dorsal fin spine; admfs, admedian fin spine; afs, anal fin spine; al, ascending lamina; alor, anterior lorical plate; bst, branchiostegal plates; pdfs, posterior dorsal fin spine; pelfs, pelvic fin spines; ppelfs1–3, prepelvic fin spines 1–4; ppms, pfs, pot, postorbital tessera; pi, pinnal

plate; pps, prepectoral spines; sp, sclerotic plates; tt, tectal tesserae; vl, ventral lamina. Scale bars, 1 mm.

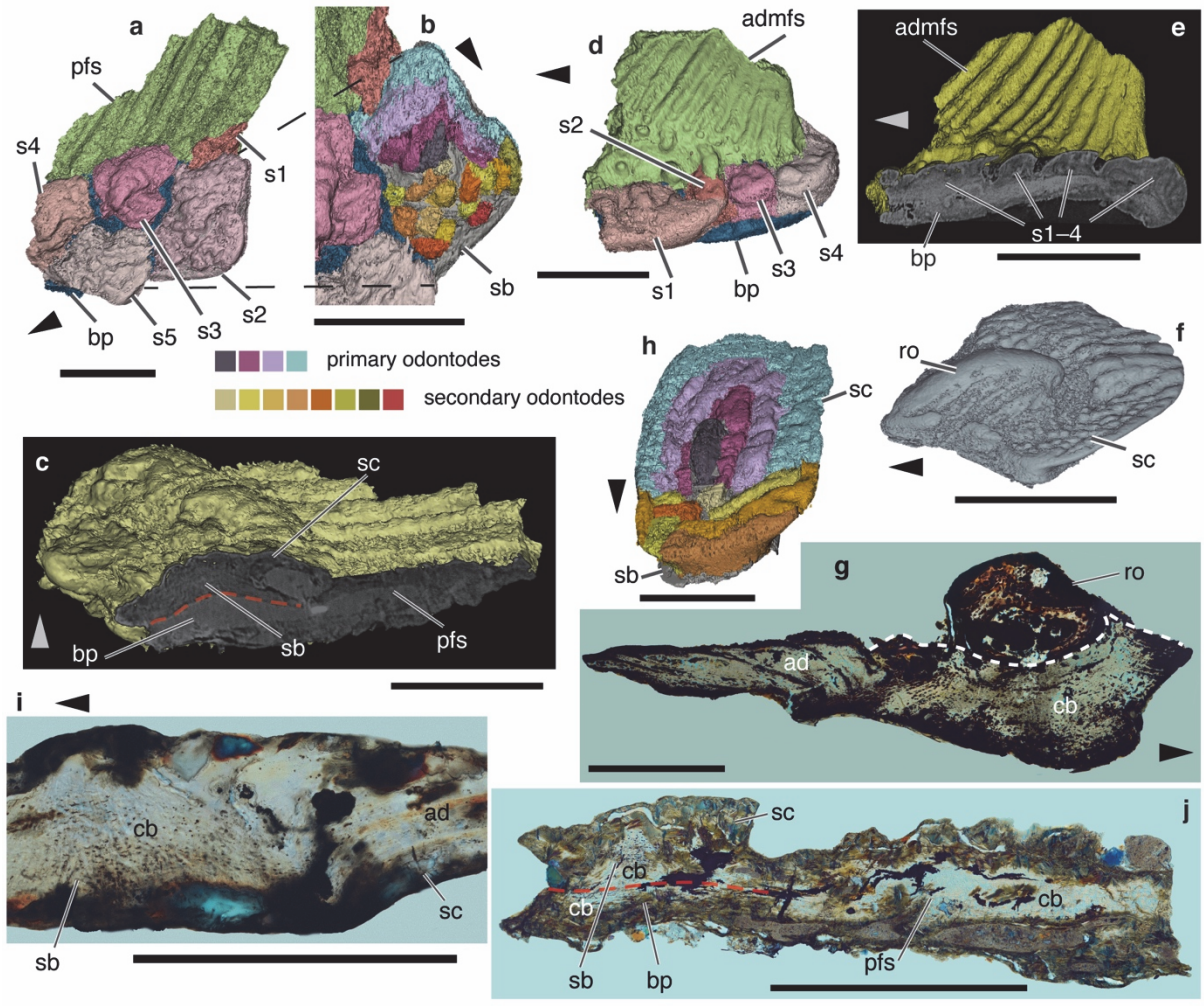

Fig. 2 | Histological and developmental features of the pectoral shoulder girdle and trunk scales of *Fanjingshania renovata.* Volume renderings generated from X-ray synchrotron (a–e) and microcomputed tomography (f, h) data and optical micrographs (g, i, j). **a**, A fragment of a pectoral fin spine fused to a partial ventral lamina of a pinnal plate depicted in external (ventral) view (V27433.1, holotype). **b**, Detail of a pinnal plate scale (s2) in V27433.1 with colour-coded secondary and primary odontodes. **c**, Virtual slice through the pinnal plate and pectoral fin spine wall of the holotype (V27433.1). **d**, Lateral view of an incomplete admedian fin spine fused to a fragment of pinnal ventral lamina (V27434.1). **e**, Virtual slice through the partial pinnal plate of V27434.1. **f**, Lateral crown aspect of a trunk scale with a large replacement odontode (V27435.2). **g**, Longitudinal section of an isolated trunk scale with an anterior replacement odontode (V27435.5). **h**, Asymmetrical trunk scale (V27435.1) in anterior crown view. i, Part of a longitudinally sectioned trunk scale (V27435.22). **j**, Section through a partial pinnal plate fused to a fragment of pectoral spine wall (V27433.2). Squares correspond to colour-coded odontodes in (b) and (h). Red dashed lines mark scale base/basal plate boundary. White dashed lines mark resorption surfaces. ad, atubular dentine; admfs, admedian fin spine; bp, basal plate; cb, cellular bone; pfs, pectoral fin spine; pi, pinnal plate; ro, replacement odontode; sb, scale base; s1–5, scale 1–5; sc, scale crown. Scale bars, 1mm (a–f, h, j), 0.5 mm (g, i).

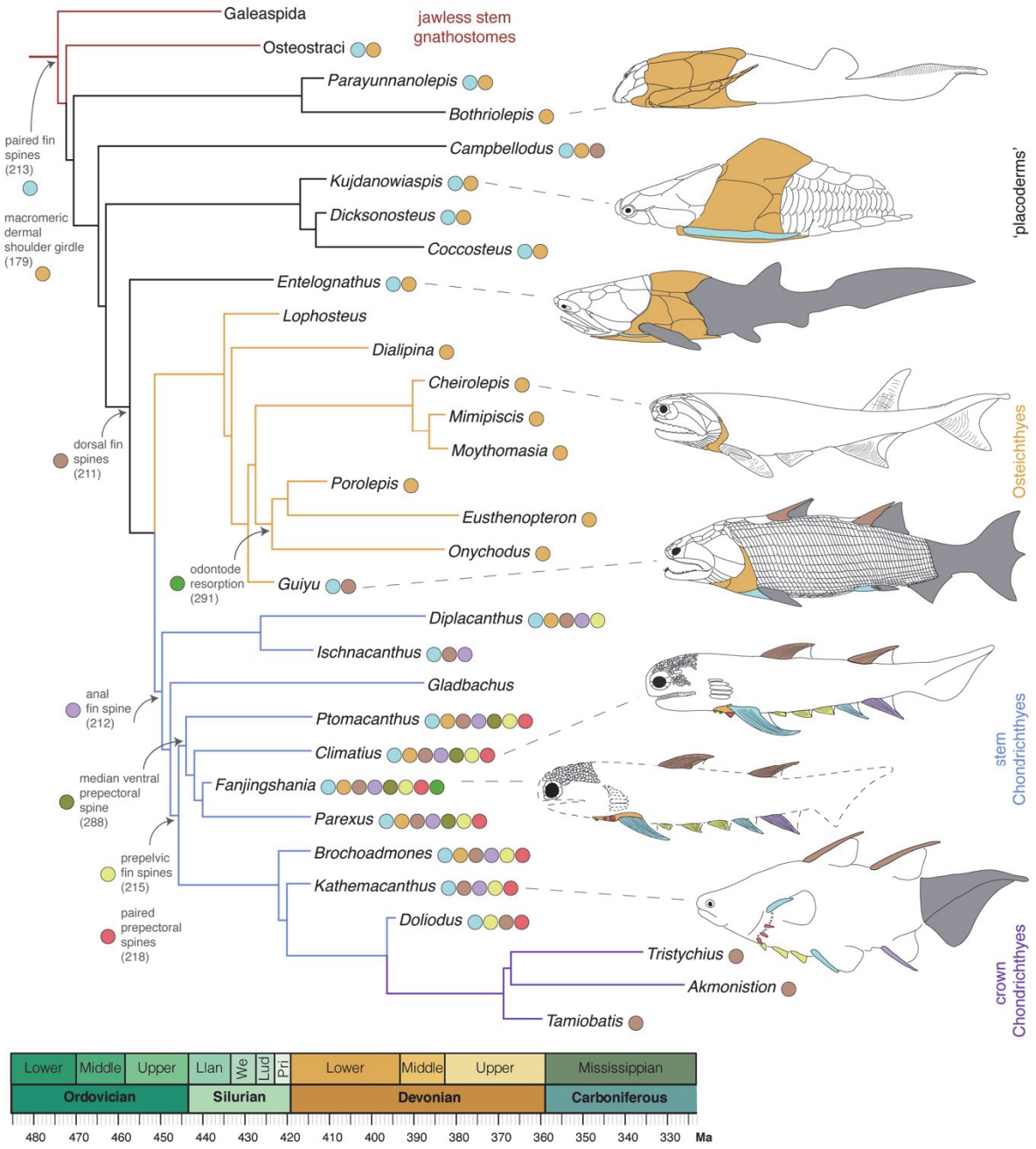

582

583 **Fig. 3 | Phylogenetic placement of *Fanjingshania renovata* within early jawed vertebrates.**
584 Simplified 50 percent majority-rule consensus tree from a parsimony analysis of a data matrix of 105
585 taxa and 292 characters. Diagrams to the right of the tree illustrate the distribution of dermoskeletal
586 characters possessed by *Fanjingshania* in select chondrichthyans, osteichthyans and 'placoderms'
587 (see also Supplementary Information). Circles at internal nodes represent parsimony reconstructions
588 of a select set of anatomical and developmental/histological characters coded for *Fanjingshania*.
589 Circles opposite taxon labels show presence of these characters at terminal nodes. Character number
590 in the data matrix is given in parentheses (see Supplementary Information).

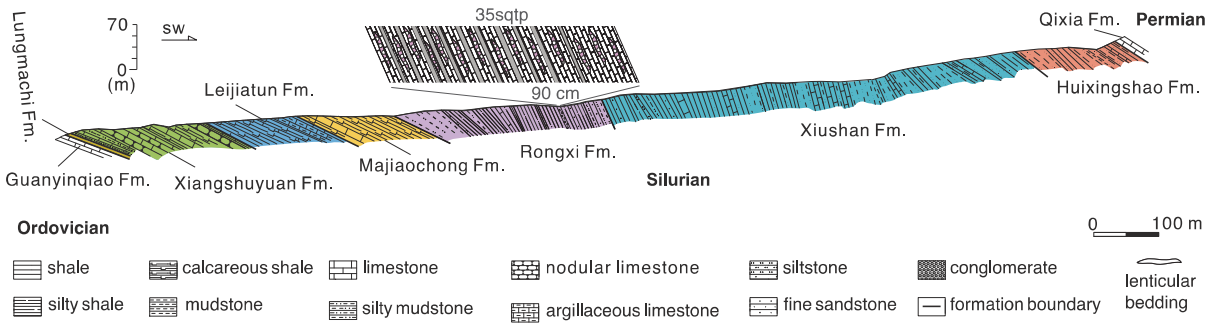

591

592 **Extended Data Fig. 1 | The Shiqian-Tunping section at Leijiatun (Shiqian County, Guizhou**
593 **Province, China).** Diagram revealing the relationship of the Rongxi to the other Silurian
594 lithostratigraphic units (color coded) exposed at Shiqian-Tunping and the location of the
595 *Fanjingshania*-bearing beds (depicted in grey, sample 35SQTP) within the sequence.

596

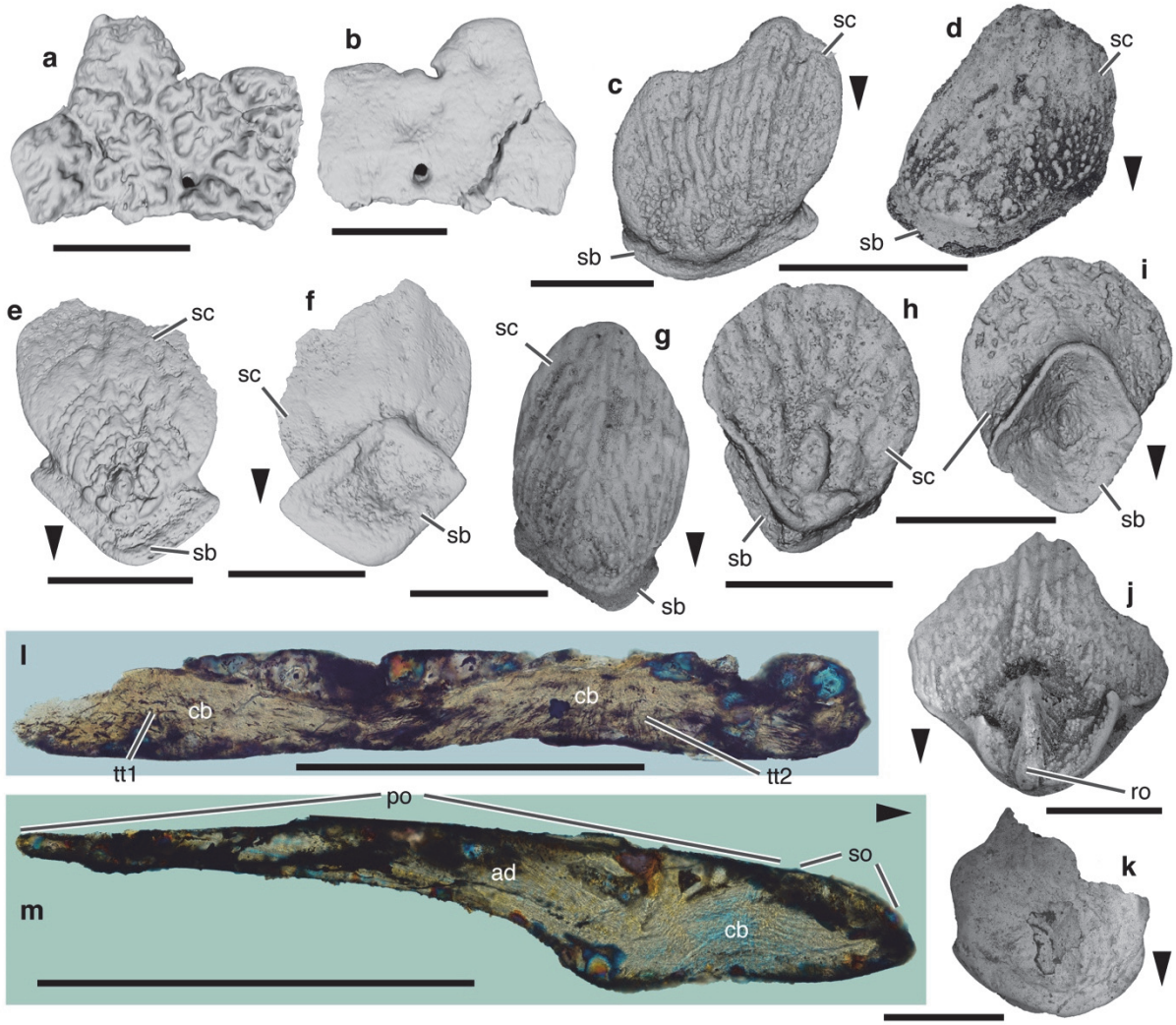

Extended Data Fig. 2 | Head and trunk dermoskeletal elements of *Fanjingshania renovata*. Volume renderings based on X-ray microcomputed tomography data (a–c, i, j, l, m), scanning electron micrographs (d, k, n, o) and optical micrographs (p, q). Fused tectal tesserae (V27438.4) in **a**, crown and **b**, basal views. **c**, Broad asymmetrical trunk scale in crown view (V27435.23). **d**, Asymmetrical trunk scale (V27435.6) in crown view. Incomplete symmetrical trunk scale (V27435.7) in **e**, crown and **f**, base views. **g**, Crown view of an asymmetrical trunk scale (V27435.12). **h**, Crown view of a symmetrical trunk scale (V27435.24) with a large anterior tubercle. **i**, Basal view of V27435.24. **j**, Crown view of a trunk scale (V27435.11) with an anterior replacement odontode. **k**, Incomplete trunk scale (V27435.9) with an anteriorly excavated crown. **l**, Section through two fused tectal tesserae (V27438.5)**. m**, Longitudinal section through a trunk scale (V27435.8). Arrowheads point to anterior. ad, atubular dentine; cb, cellular bone; po, primary odontodes; ro, replacement odontode; sb, scale base; sc, scale crown; so, secondary odontodes, tt, tectal tesserae. Scale bars, 1mm.

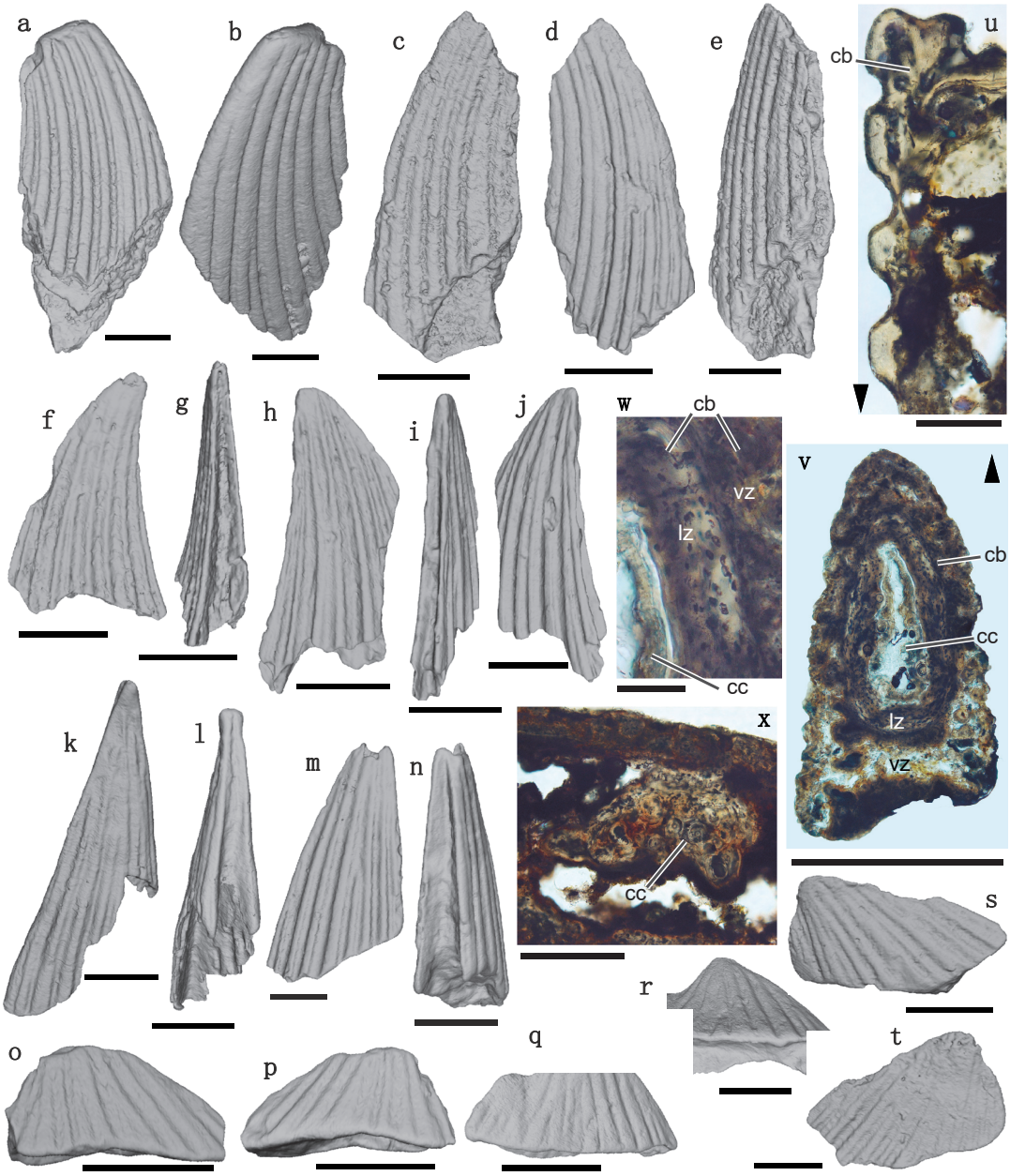

Extended Data Fig. 3 | Fin spines of *Fanjingshania renovata*. Volume renderings based on X-ray microcomputed tomography data (a–t) and optical micrographs (u–x). Incomplete pectoral fin spine (V27437.9) in **a**, lateral and **b**, apical lateral view. Incomplete pectoral spine (V27437.10) in (**c**, **d**) lateral and **e**, posterior lateral views. Pelvic fin spine (V27437.11) in **f**, lateral and **g**, posterior views. Partial anterior dorsal fin spine (V27437.12) in (**h**, **j**) and **i**, posterior views. Incomplete posterior dorsal fin spine (V27437.13) in **k**, lateral and **l**, posterior views. Incomplete anal fin spine (V27437.14) in **m**, lateral and **n**, posterior views. (**o**, **p**) Incomplete prepelvic fin spine (V27441.4) in lateral views. Prepelvic fin spine (V27441.5) in **q**, lateral and **r**, basal lateral views. (**s**, **t**) Incomplete prepelvic fin spine (V27441.6) in lateral apical views. **u**, Transversely sectioned fin spine fragment (V27437.2) shown in part. **v**, Transversely sectioned apical fragment of a fin spine (V27437.1). **w**, Enlarged anterior of **v**, showing detail of the spine's tissue structure. Portion of a longitudinally sectioned pectoral fin spine (V27437.14). cc, calcified cartilage; cb, cellular bone; lz, lamellar zone; vz, vascular zone. Scale bars, 1mm (a–t), 0.5 mm (v), 0.25 mm (u), 0.2 mm (x) and 0.05 mm.

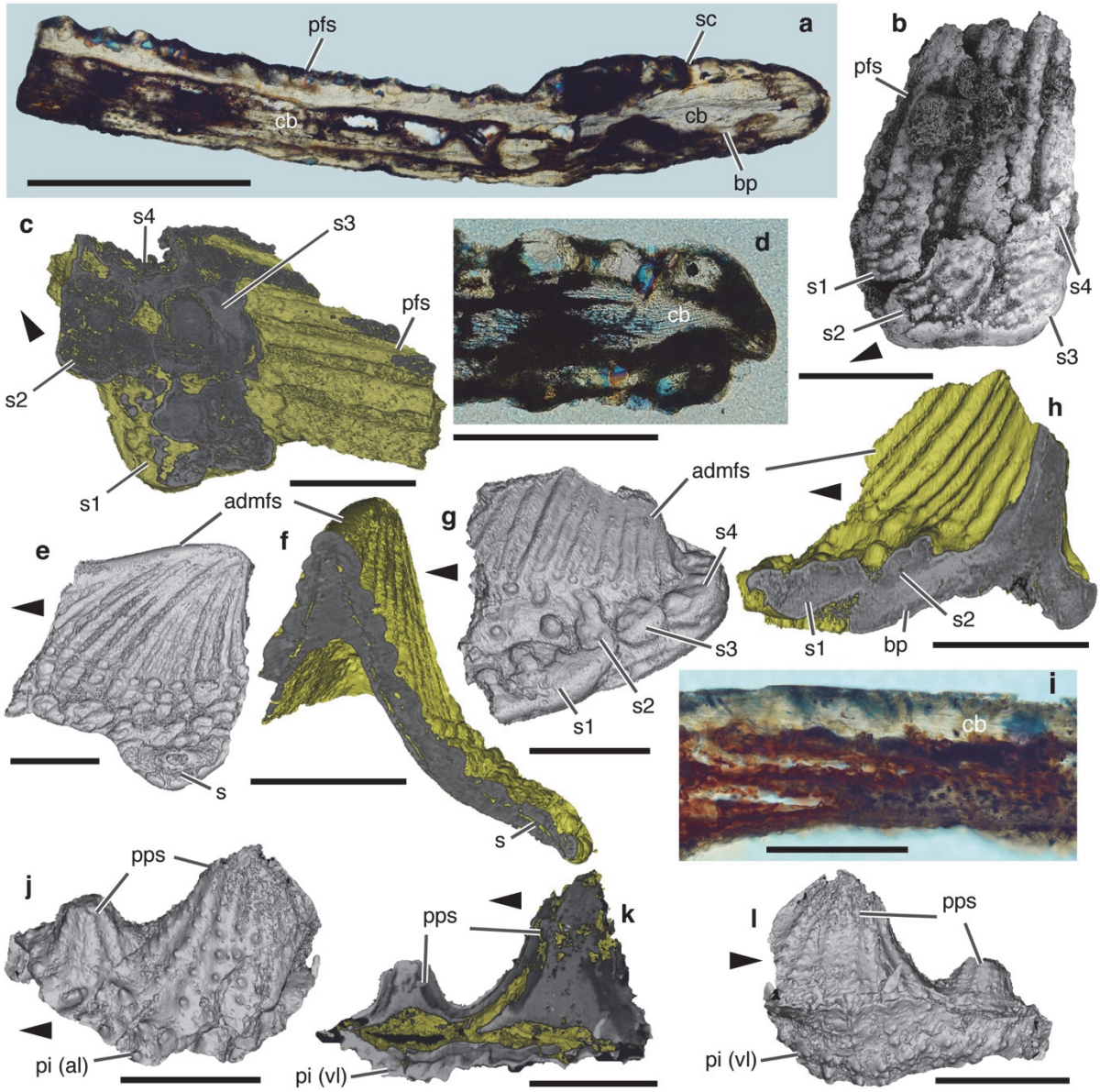

Extended Data Fig. 4 | Elements of the dermal shoulder girdle of *Fanjingshania renovata*. Optical micrographs (a, d, i), scanning electron micrograph (b) and volume renderings based on synchrotron (e–h) and microcomputed (j–l) X-ray tomography data. **a**, Section through a fragment of a pectoral fin spine wall fused to a partial pinnal plate (V27433.3). **b**, Fragment of a pectoral fin spine wall fused to a partial pinnal plate (V27433.5) in external view. **c**, Horizontal virtual section through a partial pinnal plate fused to a pectoral fin spine fragment (V27433.1, holotype). **d**, Detail of a pectoral fin spine wall (from a sectioned pectoral fin spine fragment fused to a partial pinnal plate, V27433.6). **e**, Lateral view of an admedian fin spine fused to a pinnal plate fragment (V27434.3). **f**, Transverse virtual slice through V27434.3 shown in anterior view. **g**, Lateral view of an incomplete admedian fin spine fused to a fragment of pinnal plate (V27434.1). **h**, Virtual transverse section through V27434.1 in posterior view. **i**, Portion of basal wall of an admedian fin spine (V27434.4) sectioned along its long axis, apical to the left. **j**, Lateral view of two prepectoral spines fused to a partial pinnal plate (V27436.1). **k**, Vertical virtual slice through V27436.1 in ventral view. **l**, Lateral view of V27436.1 showing ventral pinnal plate lamina (downturned due to a post-mortem fracture). **l**, Horizontal virtual slice through the prepectoral spines of V27436.1. Arrowheads point to anterior. admfs, admedian fin spine; al, ascending lamina; bp, basal plate; cb, cellular bone; pfs, pectoral fin spine; pi, pinnal plate; pps, prepectoral spines; s1–4, scales 1–4; sc, scale crown; vl, ventral lamina. Scale bars, 1 mm (a–c, e–h, j–l), 0.5 mm (d) and 0.2 mm (i).

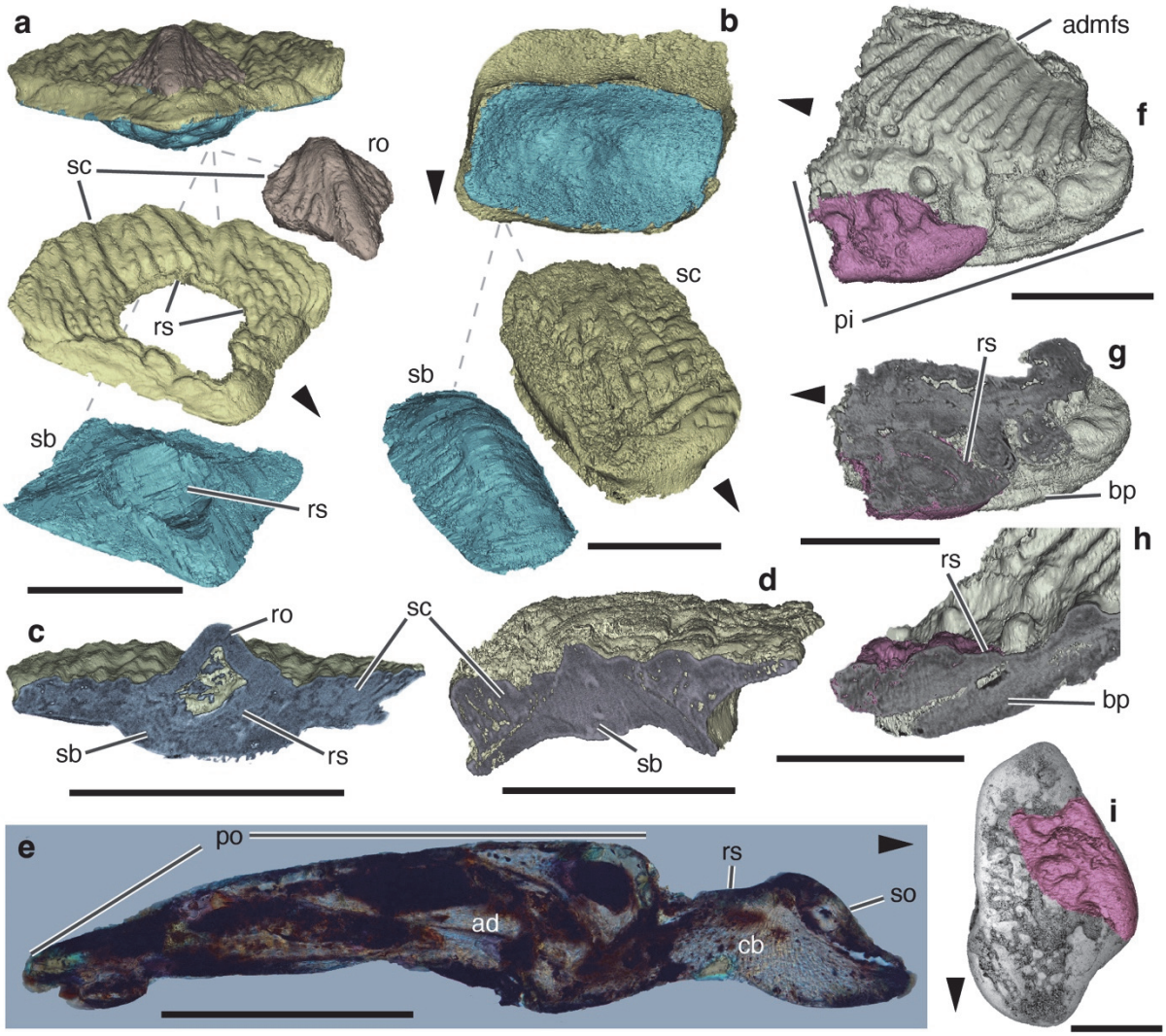

644

645 **Extended Data Fig. 5 | Resorption features in the dermal skeleton of *Fanjingshania renovata*.**,
646 Volume renderings based on synchrotron X-ray tomography data (a–d, f–i), optical micrograph (e)
647 and scanning electron micrograph (i). **a**, Trunk scale (V27435.10) with an anterior replacement
648 odontode and 'exploded view' of the same specimen revealing the resorption surfaces in the scale
649 crown and base. **b**, Basal view of an asymmetrical trunk scale (V27435.1) and the crown and base of
650 the same specimen in crown aspect demonstrating absence of resorption surfaces in contrast to
651 V27435.10. **c**, Transverse virtual slice through V27435.10 at the level of the replacement odontode. **d**,
652 Transverse virtual slice through V27435.1 at the level of the primordial odontode. **e**, Longitudinally
653 sectioned trunk scale (V27435.4) with an anterior resorption surface. **f**, A partially resorbed pinnal
654 plate scale highlighted in a dermal shoulder girdle fragment (V27433.1, partial admedian fin spine
655 fused to a fragment of a pinnal plate) shown in external (ventral) view. **g**, Horizontal virtual slice
656 through the pinnal plate and fin spine wall of V27433.1. **h**, Vertical virtual slice through the pinnal plate
657 and fin spine wall of V27433.1. **i**, Partially resorbed pinnal plate scale shown in (f–h) superimposed
658 onto an isolated trunk scale (V27435. 27). Image of resorbed scale reflected and magnified 1.5x the
659 scale in (i). ad, atubular dentine; admfs, admedian fin spine; bp, basal plate; cb, cellular bone; pi,
660 pinnal plate; po, primary odontodes; ro, replacement odontode; rs, resorption surface; sb, scale base;
661 sc, scale crown; so, secondary odontodes. Scale bars, 1 mm (a–d, f–i) and 0.5 mm (e).

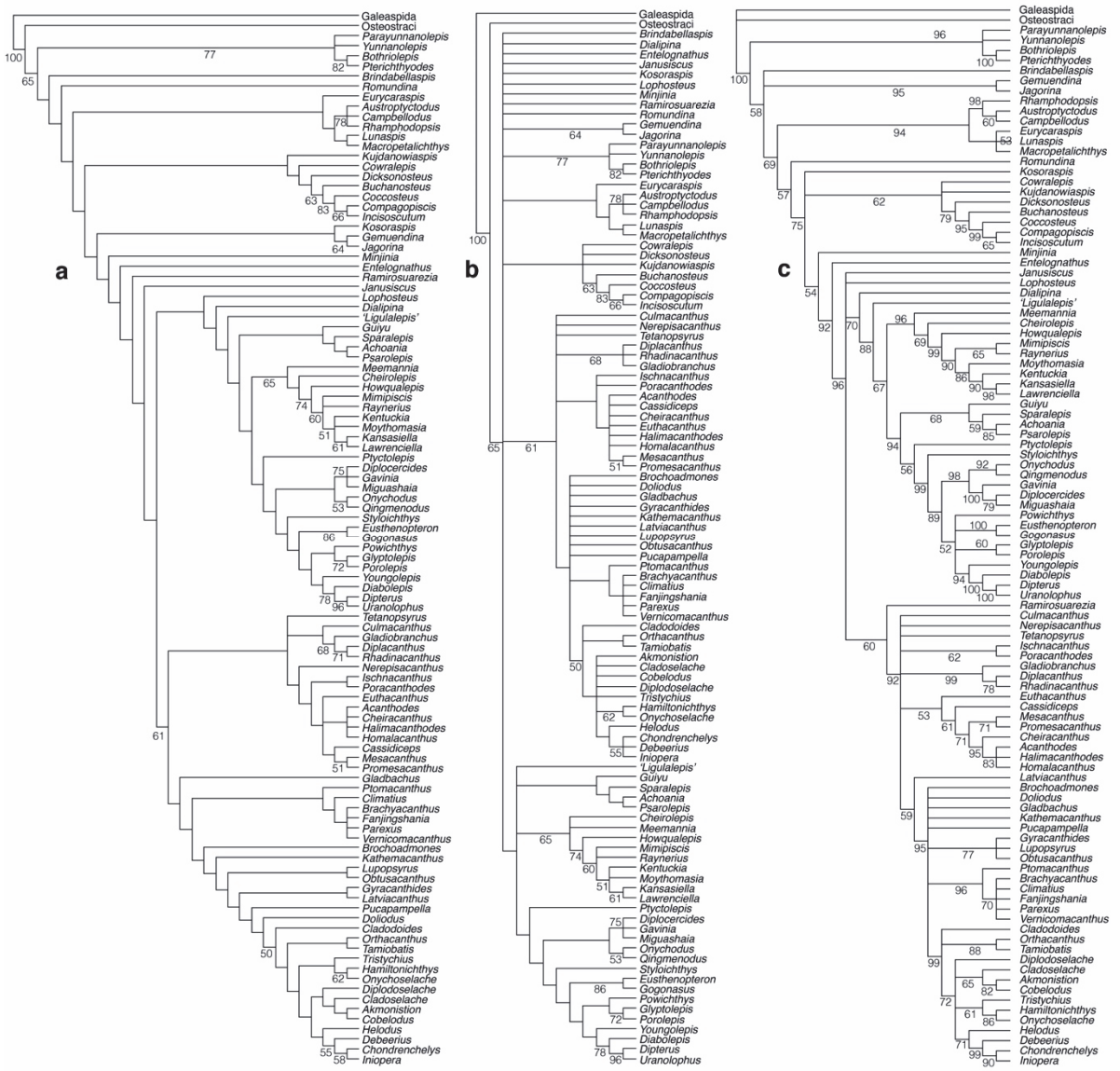

Extended Data Fig. 6 | Phylogenetic reconstructions of early gnathostomes based on a data matrix of 105 taxa and 292 characters. a, 50 percent majority-rule and **b**, strict consensus trees from an analysis performed under parsimony optimality criteria (numbers in (a) and (b) represent 50 percent and above bootstrap support for internal nodes). **c**, 50 percent majority-rule consensus tree from a Bayesian phylogenetic analysis (numbers represent posterior probability values).

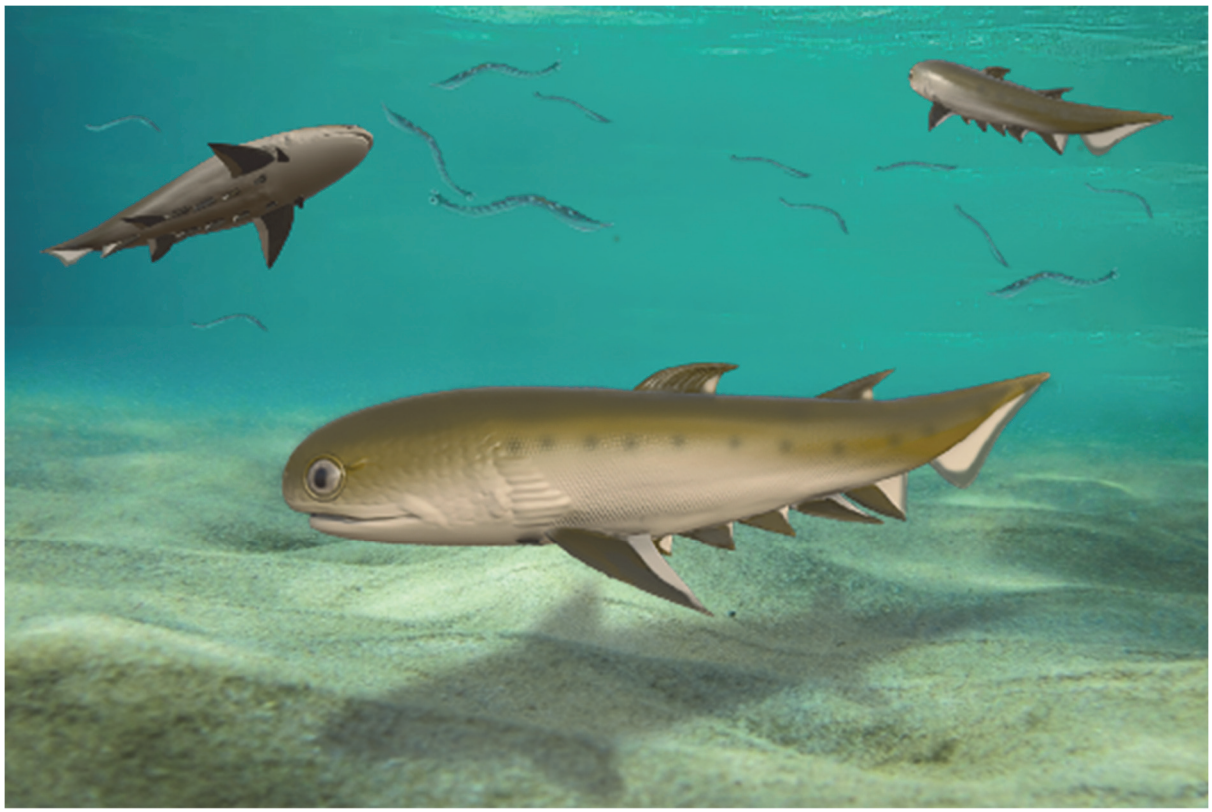

Extended Data Fig. 7 | **Life reconstruction of *Fanjingshania renovata*.** Artwork by Fu Boyuan and Fu Baozhong.

672 **Supplementary Information for:**

673 Spiny chondrichthyan from the lower Silurian of South
674 China

675 Plamen S. Andreev1,2†, Ivan J. Sansom3†, Qiang Li1,2†, Wenjin Zhao2,4,5, Jianhua
676 Wang1, Chun-Chieh Wang6, Lijian Peng1, Liantao Jia2, Tuo Qiao2,4, Min Zhu2,4,5*

677 1Research Center of Natural History and Culture, Qujing Normal University, Qujing 655011,
678 Yunnan Province, China. 2Key CAS Laboratory of Vertebrate Evolution and Human Origins,
679 Institute of Vertebrate Paleontology and Paleoanthropology, Chinese Academy of Sciences
680 (CAS), Beijing 100044, China. 3School of Geography, Earth and Environmental Sciences,
681 University of Birmingham, UK. 4CAS Center for Excellence in Life and Paleoenvironment,
682 Beijing 100044, China. 5University of Chinese Academy of Sciences, Beijing 100049, China.
683 6National Synchrotron Radiation Research Center, Hsinchu 30076, Taiwan.

684 *Corresponding author: zhumin@ivpp.ac.cn.

685 †These authors contributed equally to this work.

686

Horizon and locality

Vertebrate-bearing samples (35SQTP) containing the *Fanjingshania* material were collected from a recently exposed road section (Shiqian-Tunping) of the Rongxi Formation[1,2] located near the village of Leijiatun in Shiqian County, Guizhou Province, China. The samples come from a unit of interbedded mudstone and limestone conglomerate beds from the upper part of the Rongxi Formation (Extended Data Fig. 1). Present in 35SQTP are also platform elements of the conodont *Ozarkodina guizhouensis*[3] that is indicative of the upper Aeronian–lower Telychian *Ozarkodina guizhouensis* Biozone[1,4]. The Rongxi Formation at Shiqian has been dated to the upper Aeronian, within the *Ozarkodina parahassi* division of the *O. guizhouensis* Biozone, using biostratigraphic evidence from the underlying Majiaochong and the overlying Xiushan Formations[5,6]. Alternative, lower Telychian, age estimates[1] can be explained by the recently proposed diachronous nature of the Rongxi Formation at localities across South China[4]. We therefore consider the Aeronian age of the Rongxi Formation as most plausible.

Specimen descriptions

Holotype. Isolated specimen (V27433.1) preserving a fragment of a spine wall fused along its basal margin to articulated dermal scales supported by a basal plate (Fig. 2a, c and Extended Data Figs. 4c, 5a–c). The exterior surface of the partial spine is ornamented by six tubercle-studded ridges of varying width. The ridges are flat-topped with scalloped lateral sides and extend to contact the scales at an acute angle (Figs. 1g, 2a). The spine preserves an undamaged posterior edge that bears a deep longitudinal indentation. Surface renderings and virtual slices reveal in situ

711 fusion of scale bases by a common basal plate. The latter is best preserved in the
712 posterior of the specimen where it is seen to be continuous with the inner portion of
713 the spine wall (Fig. 2c). The scales have a staggered arrangement, forming an
714 anterior (incompletely preserved) and posterior pairs oriented obliquely in relation to
715 the spine base (Fig. 2a). A partial scale is present between the posterior-most spine
716 ridge and the scale pairs (Fig. 2a). Scale crowns have a rhomboid appearance and
717 possess irregular margins accentuated by an enlarged lateral lobe. The crown
718 surfaces show signs of post-mortem abrasion and preserve deep grooves separating
719 high relief nodose ridges. A prominent button-shaped tubercle is a consistent feature
720 of the crown anterior where the ornament changes to disorganised short ridges and
721 tubercles. Volumetric reconstructions reveal concave scale bases with low profiles
722 that do not extend beyond the crown margins.

723 The tomography data demonstrate a clear density contrast between the tissue
724 of the basal plate and the more radiotransparent scales fused to it (Fig. 2c). The
725 basal plate extends to occupy the spaces between the scales and is continuous with
726 the inner portion of the spine wall (Fig. 2c and Extended Data Figs. 4c, 5h).
727 Radiopaque material is present inside the spine ridges whose tissue displays a faint
728 lamellar texture in horizontal virtual slices (Fig. 2c and Extended Data Fig. 4c).
729 Scales possess compound crowns of appositionally deposited odontode generations
730 of increasingly larger size (Fig. 2b). The crowns' primordial odontode surmounts the
731 apex of the base and is bounded anteriorly by a cluster of vermiform and tuberculate
732 secondary odontodes. Scale bases consist of lamellar bone with plywood-like
733 architecture pervaded by vertically oriented fibres (Fig. 2c). In the partial scale, the
734 crown and base are truncated by irregular resorption surfaces along which the scale
735 makes contact with the spine (Fig. 2b).

736

737 **Other fused elements.** Represented by incomplete shoulder girdle plates fused to
738 spines and spine fragments, fused sclerotic plates and fused head tesserae.

739 *Type 1 dermal elements (partial pectoral fin spines fused to fragments of a pinnal*
740 *plates).* These constitute partial spine bases fused to a basal plate carrying dermal
741 scales of the type possessed by the holotype. Investigated specimens (V27433.1–
742 V27433.9) preserve up to 13 spine ridges of variable width adorned by nodose
743 ornament (Fig. 1t and Extended Data Fig. 4b). The spine wall of these is either level
744 with (Fig. 2c, j) or joins at an angle (Fig. 1t and Extended Data Fig. 4a) the basal
745 plate/scales units. Specimens of the latter type show fragmentation of the spine's
746 ridged ornament into strings of independent nodes (Fig. 1t) near the contact with the
747 base.

748 The plates' scales arrange with an offset and organise in rows that are
749 directed obliquely relative to the spine ridges. As observed in the holotype, some of
750 the scales proximal to the spine represent resorbed remnants of regular-sized scales
751 exhibiting truncated crown ornament along a ruffled longitudinal margin facing the
752 spine (Extended Data Fig. 4b). In some specimens the spine ridges develop
753 between the proximal scales or even extend beyond their anterior edge. Scale
754 crowns are asymmetrical with ovoid to rhomboid appearance and possess an
755 ornament of prominent nodose ridges that anteriorly become discontinuous and
756 organise around a conspicuous medial pustule. In less abraded specimens the
757 crown surface is studded with tubercles formed on top of the main sculpting features.

758 Thin-sectioned specimens (V27433.2, V27433.3, V27433.6 and V27433.7)
759 demonstrate extensive diagenetic replacement of hard tissues inside scale crowns

and the nodose sculpture of the spine ridges (Fig. 2j and Extended Data Fig. 4a, d). Optically faint depositional lines and rudiments of pulp canals are however preserved in the scale crowns of V27433.3 (Extended Data Fig. 4a). Other sectioned material (V27433.2 and V27433.7) shows evidence of partial and/or complete removal of odontodes and basal tissue along the oblique resorption surfaces of partial scales. Scale bases consist of compact lamellar bone harbouring fusiform cell lacunae and vertically oriented fibre spaces (Fig. 2j and Extended Data Fig. 4a, d). The lamellar bone continues below the bases without an optically distinct boundary and forms a basal palate that fuses the scales together. It also extends into the inner spine wall with no break in its lamellar structure. The same tissue architecture is maintained across the thickness of the spine wall, including inside the ornamenting ridges. Similar to the lamellar bone of the scale bases and basal plate, the tissue exhibits flattened cell lacunae and fibre spaces directed orthogonal to the spine's outer surface (Extended Data Fig. 4d).

Type 2 dermal elements (complete and partially preserved admendian spines fused to pinnal plate fragments). Specimens consisting of a low, laterally compressed spine with a broad elliptical base fused to a partial dermal lamina (Figs. 1c, d, 2d, e, and Extended Data Fig. 4e–i). The spine apex is posteriorly offset due to an acutely angled anterior margin that bears a strong keel connected to an ornament of equally spaced nodose ridges. The posterior spine edge has a slightly concave, near vertical profile and does not develop a noticeable longitudinal sulcus. Around its perimeter the spine base flares out into a shelf-like extension where the ornamenting ridges fragment into series of individual nodes. The examined fragmentary material demonstrates ovoid or kidney-shaped scales (Fig. 2d and Extended Data Fig. 4g) fused to the lateral and/or posterior margins of spine bases. In less abraded

specimens (Fig. 1d) the scale crowns are ornamented by tuberculate ridges aligned in an antero-posterior direction. Some of the scales in contact with the spine wall possess crowns truncated by irregular resorption surfaces developed primarily along their long axis. All scales fuse to a basal plate with irregular outer margins that follows the scales' contour and is clearly delineated from them around its periphery by a recessed border.

A longitudinally sectioned specimen preserves a portion of the original structure of the outer spine wall where a lamellar bone is identified to harbour fusiform cell lacunae aligned with the tissue's lamellae (Extended Data Fig. 4i). Tomographic slices show this outer zone of the spine to be pervaded by a vascular network of canals present inside the ornamenting ridges as well deeper within the tissue (Extended Data Fig. 4f). In V27434.3 the vascular zone is separated internally by a radiotransparent boundary from a compact tissue developed in the apical portion of the spine (Extended Data Fig. 4f). The lamellar bone of the spine wall extends to form the basal plate that fuses together the scales to the spine periphery. This lamellar architecture is also developed inside the scale bases with a perceptible change in radiodensity marking the transition between the two in V27434.1 (Extended Data Fig. 4h). A prominent pustule-shaped crown primordium surmounts the base apically and is the first in a row of appositionally deposited primary odontodes (Fig. 2e). A smaller component of the scale crowns is a cluster of vermiform secondary odontodes deposited anteriorly and laterally to the primordium. Many of the scales in proximity of the spine wall are in various stages of resorption evidenced in the synchrotron data by irregular surfaces truncating the odontode generations (Fig.2d, e and Extended Data Figs. 4g, h).

Type 3 dermal elements (prepectoral spines fused to pinnal plate fragments). Two specimens (V27436.1 and V27436.2) possessing a pair of spines of unequal size that fused laterally to partially preserved dermal plates (Fig. 1c, d and Extended Data Fig. 4j–l). The spines are squat, laterally flattened and near symmetrical elements fused together along their long axes. The larger of the two spines shows a slight bend towards one of its lateral sides. Both spines possess ridged ornament that is continuous with rows of tubercules carried by the dermal plate laminae. In either specimen, intact plate margins are preserved only on one side of the spines and demonstrate an undulating edge indented by a deep uninterrupted groove as well as broadening of the plate in direction of the larger spine.

Tomography data from V27436.1 show fusion of the spine walls at their bases as well as canal spaces rimmed by concentric depositional lines formed within the ornamenting ridges and deep inside the spine wall.

Type 4 dermal element (anterior lorical plate fused to a median prepectoral spine). A single specimen comprising of a diminutive spine fused to a partially preserved basal plate (Fig. 1p). The spine has a stubby, conical appearance with nodose ridges radiating down from its apex. Around most of its circumference the spine is fused to a fragment of a basal plate bearing a coarse tuberculate ornament. Only one of the plate's free margins is largely intact and demonstrates a recessed edge arched into a prominent medial bulge that aligns with the spine. Preserved portions of the basal plate flanking the spine also possess deeply grooved margins and carry partial scale crowns ornamented with disjointed ridges and tubercles.

Type 5 dermal elements (fused sclerotic plates). A single specimen (Fig. 1r) displaying one partial and one complete plate with curved profiles fused along a

linear contact surface. A fragment of a third element is fused to each of the better preserved plates. The complete plate is polygonal and possesses a dome-like raised area that is located near its junction with the partial plate where a similar acuminate region is also present. The plates possess an ornament of thick radiating ridges that descend from their apical areas and become discontinuous towards the periphery. One side of the plates' margins is shaped into a well-defined, continuous arc with a characteristic 'lip' not developed elsewhere around their perimeter. The visceral surface of the complete plate is concave and divided longitudinally by a low ridge.

Type 6 dermal elements (fused tectal tesserae). Six specimens representing fused in articulation polygonal tesserae exhibiting flattened profiles and planar lower surfaces. The largest of these aggregates consists of 8 tesserae (Extended Data Fig. 2a, b) of varying sizes and shapes adorned by branching ridges anastomosing to a medial ridge. Differences in tessera shape and size are also observed in compound two- and three-tessera elements.

A thin-sectioned specimen (Extended Data Fig. 2l) comprising of two fused tesserae reveals basal lamellar bone harbouring cell lacunae aligned with the tissue's lamellae. The base is pervaded by extrinsic fibre space that converge towards its apex. Histological detail of tessera crowns is lacking due to extensive diagenetic alteration of original tissue structure.

Disarticulated material

Spine morphology A (pectoral fin spines). Incomplete specimens (Fig. 1e, f and Extended Data Fig. 3a–e) constituting laterally compressed, elongate *s*pines with broad sides and strongly recurved profiles. The spines exhibit a gradual apical taper accompanied by apical convergence of the spine ornament. The latter is developed

on the spines' lateral sides as flat-topped nodose ridges of variable width that bifurcate basally. In non-abraded specimens (Fig. 1e) the ridges are studded with fine tubercles also present on the anterior spine edge where they are carried on an enlarged rib-like ridge. A deep sulcus runs the length of the posterior spine edge.

The wall of pectoral and other fin spine morphologies consists of a cellular bone tissue organised into an outer vascular and inner lamellar zone (Extended Data Fig. 3v, w). The thicker outer zone is extensively recrystalised in all examined specimens and contains diagenetically infilled canals running parallel the spine surface (Extended Data Fig. 3u, v). Concentric deposition of the cellular bone around the canals is identified optically in thin sectioned spines. The inner zone has a compact appearance and harbours densely packed fusiform cell spaces infilled by optically opaque diagenetic material (Extended Data Fig. 3w). The cell spaces align with the bone lamellae of the inner zone tissue that arrange circumferentially around the spine core. Apically, the central spine cavity is occupied by calcified cartilage consisting of aggregates of mineralised globules and wavy growth increments (Extended Data Fig. 3w, x). Arrested growth surfaces are evident in globules in contact with the inner cellular bone.

Spine morphology B (pelvic fin spines). Partial and nearly complete spines (Fig. 1h, i and Extended Data Fig. 3f, g) with acuminate, moderately arched profiles and flattened lateral sides. Some specimens preserve the basal portion of the spine that broadens noticeably in respect to its apical part (Fig. 1h, i). Flat-topped nodose ridges of varying width adorn the spines' lateral sides with some of the ridges bifurcating in proximity of the spine base. A progressively widening and deeply incised sulcus marks the posterior spine edge.

Spine morphology C (anterior dorsal fin spines). Represented by incomplete spines (Fig. 1n, o and Extended Data Fig. 3h–j) exhibiting extreme lateral compression and broad profiles with an arched anterior and slightly curved posterior margins. The spines' lateral sides bear ornamenting ridges of the kind recorded in morphologies A and B and a posterior sulcus along the length of preserved portions of specimens.

Spine morphology D (posterior dorsal fin spines). Partially preserved acuminate spines (Fig. 1l, m and Extended Data Fig. 3k, l) possessing straight to lightly depressed anterior and posterior edges that diverge rapidly to form a broad base. The spines exhibit moderate lateral compaction and carry the vertical ridged ornament observed in the other spine morphologies (A to C). A deep and basally widening sulcus is present along the preserved apical portions of the spines' posterior edge. The core of the spines is occupied by a large-diameter cavity that tapers off in the apical portion of the spine.

Spine morphology E (anal fin spines). Incomplete spines demonstrating acuminate profiles with a gently arched anterior edge and a straight posterior margin (Fig. 1j, k and Extended Data Fig. 3m, n). The lateral sides of the spine trunk bear nodose ridges of variable width that bifurcate in the apical and basal portions of the spines. A basally widening sulcus is a feature of the posterior spine edge.

Spine morphology F (prepelvic fin spines). Complete and partially preserved stubby spines (Fig. 1u–w and Extended Data Fig. 3o–t) with lengths exceeding two times or more the height of their apices. The spines exhibit strong lateral compression that produces an elliptical base with a narrow footprint. Three morphological variants of these spines are distinguished on the basis of differences in the angle of slope of the anterior spine edge. Specimens with a low anterior margin possess an apex with an

905 extreme posterior offset (Fig. 1u and Extended Data Fig. 3o, p). The other two
906 variants (Fig. 1v, w and Extended Data Fig. 3q–t) have steeper anterior margins and
907 develop a diminutive accessory cusp posterior of the spine apex. Spine ornament is
908 represented by evenly spaced nodose ridges that bifurcate basally and converge
909 towards the spine apex and accessory cusps when present. Complete specimens
910 display an excavated basal surface throughout the antero-posterior length of the
911 spine.

912 *Type 7 dermal elements (a branchiostegal plate).* A plate fragment (Fig. 1q) of
913 elongate appearance preserving a wedge-shaped margin at its intact end. The
914 external plate surface carries a thick medial ridge from which radiates finer ornament
915 of nodose ridges. The visceral (basal) face of the plate is smooth and deeply
916 excavated.

917 *Type 8 dermal elements (postorbital tesserae)*. Tall and elongate tesserae with a
918 vaulted appearance possessing a wide medial crest that connects to deeply
919 engraved vertical ridges developed on their lateral sides (Fig. 1s). These ridges carry
920 secondary nodose ornament and bifurcate as well as become discontinuous in a
921 basal direction. In the figured specimen (Fig. 1s) two polygonal tectal tesserae are
922 fused to one side the periphery of the tessera.

923 *Type 9 dermal elements (isolated trunk scales).* Partially preserved and complete
924 scales (Fig. 2f, h and Extended Data Figs. 2c–k, 5a–e, i) possessing rhomboid to
925 ovoid crowns supported by a low base. The specimens display symmetrical as well
926 as asymmetrical crowns with moderate to extreme extension posterior of the scale
927 base. Crown surfaces bear elaborate ornament of fine tubercles and discontinuous
928 nodose ridges with antero-posterior alignment. The crowns' anterior develops a

conspicuous pustule-like tubercle (Extended Data Fig. 2c–e, g, h) and deep furrows that carve a complex array of vermiform ridges and tubercles (Fig. 1g and Extended Data Fig. 2d, e). In rare specimens this area of the crown and part of the underlying base are excavated by a smooth-walled depression that cuts through the surface ornament (Extended Data Figs. 2k, 5e). In a number of scales, the depression is occupied by an outsized replacement odontode that protrudes above the rest of the crown (Extended Data Figs. 2j, 5a, c). The replacement odontode is an elongate, dome-shaped element with a strong medial crest and sides ornamented by fine nodose ridges.

Scale bases have rhomboid outlines and flat or concave lower surfaces (Extended Data Figs. 2f, i, 5b, d, e). An exception to this are specimens possessing a replacement odontode where the lower base develops a conspicuous central bulge (Extended Data Fig. 5a, c).

Scale crowns consist of a row of appositionally arranged primary odontodes that increase in size in progressively more posterior positions (Extended Data Figs. 2m, 5e). Anteriorly these are bounded by vermiform and tuberculate secondary odontodes of irregular distribution (Extended Data Figs. 2c–e, g, h, m, 5e). Sectioned scales with an anterior depression reveal resorptive removal of early generations of primary and secondary odontodes as well as the apex of the scale base (Extended Data Figs. 2k, 5e). A similarly shaped resorption surface supports the large replacement odontode in all histologically examined specimens (Fig. 2g and Extended Data Fig. 5a, c).

The scale crown odontodes are formed of atubular dentine that possesses vestigial pulp cavity spaces occupied by diagenetic material. The tissue exhibits

wavy depositional lines and isolated clusters of mineralised globules (Extended Data Figs. 2m, 5e). Compact lamellar bone with closely packed cell spaces forms the scale base. Its matrix is pervaded by vertical fibre spaces that converge vertically towards the apex of the base (Extended Data Figs. 2m, 5e, d).

Remarks on the dermoskeletal characters of *Fanjingshania*

Assignment of *Fanjingshania* spine/fin spine morphologies to specific body positions is based on close similarities with the spine/fin spine complements of the climatiids (sensu Burrow et al.[7]) *Climatius*[8-10] and *Vernicomacanthus*[9,11-13]. Comparison with the head dermoskeleton of the latter two taxa, and that of another climatiid, *Brachyacanthus*[11,14], allowed to identify in *Fanjingshania* tectal and postorbital tesserae, as well as sclerotic and branchiostegal plates.

Recognition of dermal plate fragments belonging to *Fanjingshania* as pinnal and lorical plates is supported by their fusion to an array of spines and fin spines (median/paired prepectoral, pectoral and admedian). Some or all of these spine types are also documented to coalesce with paired (pinnal) and median (lorical) plates in the shoulder girdles of climatiids[7-9,15], diplacanthids[16] and other stem chondrichthyans[17]. Similar to *Fanjingshania*, histological data from *Climatius*[8] and *Diplacanthus*[16] expose pinnal and lorical plates as compound elements composed of dermal scales fused together by a basal plate.

List of characters

Abbreviations of character sources: [B] Brazeau et al.[18], [C] Coates et al.[19], [D] Dearden et al.[17] and [K] King et al.[20].

1. [B:1] **Tessellate prismatic calcified cartilage.**

0 absent

1 present

2. [B:2] **Prismatic calcified cartilage.**

0 single layered

1 multi-layered

3. [B:3] **Perichondral bone.**

0 present

1 absent

4. [B:4] **Extensive endochondral ossification.**

0 absent

1 present

5. [B:5] **Enamel(oid) present on dermal bones and scales.**

0 absent

1 present

6. [B:6] **Enamel.**

0 single-layered

1 multi-layered

7. [B:7] **Enamel layers.**

0 applied directly to one another (ganoine)

1 separated by layers of dentine

8. [B:8] **Pore canal network.**

0 absent

1 present

9. [B:9] **Dentinous tissue.**

0 absent

1 present

10. [B:10] **Dentine kind (modified).**

Character 10 of Brazeau et al.[18] was modified by introducing an extra state to account for the atubular dentine (lamellin) possessed by *Fanjingshania*.

0 mesodentine

1 semidentine

2 orthodentine

3 lamellin

11. [B:11] **Bone cell lacunae in trunk scale bases.**

0 present

1 absent

12. [B:12] **Main dentinous tissue forming fin spine.**

0 osteodentine

1 orthodentine

13. [B:13] **Longitudinal scale alignment in fin webs.**

0 absent

1 present

14. [B:14] **Differentiated lepidotrichia.**

0 absent

1 present

15. [B:15] **Composition of trunk scale crowns (modified).**

Character 15 of Brazeau et al.[18] was reformulated to describe mono- and poly-odontode scale crowns on the basis of odontode number without alluding to their patterning.

0 comprising single odontode unit/generation ("monodontode")

1 comprising a complex of multiple odontode generations/units ("polyodontode")

16. [B:16] **Concentric addition of trunk scale odontodes (modified).**

Modified character 16 of Brazeau et al.[18] distinguished from the original formulation by specifying that the concentric growth of scales refers to their odontode generations.

0 absent

1 present

17. [B:17] **Buried odontode generations (modified).**

We split character 17 of Brazeau et al.[18] in order to code separately for overgrowth of odontode generations (character 17) and odontode resorption (character 291).

0 present

1 absent

18. [B:18] **Trunk scales with peg-and-socket articulation.**

0 absent

1 present

19. [B:19] **Scale peg.**

0 broad

1 narrow

20. [B:20] **Anterodorsal process on scale.**

0 absent

1 present

21. [B:21] **Trunk scale profile.**

0 distinct crown and base demarcated by a constriction ("neck")

1 flattened

22. [B:22] **Profile of scales with constriction between crown and base.**

0 neck similar in width to crown

1 neck greatly constricted, resulting in anvil-like shape

23. [B:23] **Trunk scales with bulging base.**

0 absent

1 present

24. [B:24] **Trunk scales with flattened base.**

0 present

1 absent

25. [B:25] **Basal pore in scales.**

0 absent

1 present

26. [B:26] **Flank scale alignment.**

0 vertical rows oblique rows or hexagonal

1 rhombic packing

2 disorganised

27. [B:27] **Scute-like ridge scales (basal fulcra).**

0 absent

1 present

28. [B:28] **Sensory line canal.**

0 perforates scales

1 passes between scales

2 C-shaped scales

29. [B:29] **Dermal ornamentation.**

0 smooth

1 parallel, vermiform ridges

2 concentric ridges

3 tuberculate

30. [B:30] **Sensory line network.**

0 preserved as open grooves (sulci) in dermal bones

1 sensory lines pass through canals in dermal bones (open as pores)

31. [B:31] **Sensory canals/grooves.**

0 contained within the thickness of dermal bones

1 contained in prominent ridges on visceral surface of bone

32. [B:32] **Jugal portion of infraorbital canal joins supramaxillary canal.**

0 present

1 absent

33. [B:33] **Dermal skull roof (modified).**

State 2 was added from character 25 of Coates el al.[19]

0 includes large dermal plates

1 consists of undifferentiated plates, tesserae or scales

2 naked or largely scale free

34. [B:34] **Anterior pit line of dermal skull roof.**

0 absent

1 present

35. [B:35] **Tessera morphology.**

0 large interlocking polygonal plates

1 microsquamose, not larger than trunk squamation

36. [B:36] **Cranial spines.**

0 absent

1 present

37. [B:37] **Cranial spines.**

0 monocuspid

1 multicupsid

38. [B:38] **Extent of dermatocranial cover.**

0 complete

1 incomplete (limited to skull roof)

39. [B:39] **Openings for endolymphatic ducts in dermal skull roof.**

0 present

1 absent

40. [B:40] **Endolymphatic ducts with oblique course through dermal skull bones.**

0 absent

1 present

41. [B:41] **Endolymphatic duct relationship to median skull roof bone (i.e. nuchal plate).**

0 within median bone

1 on bones flanking the median bone (e.g. paranuchals)

42. [B:42] **Pineal opening perforation in dermal skull roof.**

0 present

1 absent

43. [B:43] **Dermal plate associated with pineal eminence or foramen.**

0 contributes to orbital margin (plate(s) excluded from orbital margin by skull roofing bones.)

1 plate bordered laterally by skull roofing bones

44. [B:44] **Broad supraorbital vaults.**

0 absent

1 present

45. [B:45] **Median commissure between supraorbital sensory lines.**

0 absent

1 present

46. [B:46] **Dermal cranial joint at level of sphenoid-otic junction.**

0 absent

1 present

47. [B:47] **Otic canal extends through postparietals.**

0 absent

1 present

48. [B:48] **Number of bones of skull roof lateral to postparietals.**

0 two

1 one

2 more than two

49. [B:49] **Suture between paired skull roofing bones (centrals of placoderms postparietals of osteichthyans).**

0 straight

1 sinusoidal

50. [B:50] **Medial processes of paranuchal wrapping posterolateral corners of nuchal plate.**

0 absent

1 present

51. [B:51] **Paired pits on ventral surface of nuchal plate.**

0 absent

1 present

52. [B:52] **Sclerotic ring.**

0 absent

1 present

53. [B:53] **Consolidated cheek plates.**

0 absent

1 present

54. [B:54] **Cheek plate.**

0 undivided

1 divided (i.e., squamosal and preopercular)

55. [B:55] **Subsquamosals in taxa with divided cheek.**

0 absent

1 present

56. [B:56] **Preopercular shape.**

0 rhombic

1 bar-shaped

57. [B:57] **Vertical canal associated with preopercular/suborbital canal.**

0 absent

1 present

58. [B:58] **Enlarged postorbital tessera separate from orbital series.**

0 absent

1 present

59. [B:59] **Extent of maxilla along cheek.**

0 to posterior margin of cheek

1 cheek bones exclude maxilla from posterior margin of cheek

60. [B:60] **Dermal neck joint.**

0 overlap

1 ginglymoid (‘arthrodire’-type)

2 reverse ginglymoid (‘antiarch’-type)

3 longitudinal

61. [B:61] **Sensory line scales/plates on head.**

0 unspecialized

1 apposed growth

2 paralleling canal

3 semicylindrical C-shaped ring scales

62. [B:62] **Bony hyoidean gill-cover series (branchiostegals).**

0 absent

1 present

63. [B:63] **Branchiostegal plate series along ventral margin of lower jaw.**

0 absent

1 present

64. [B:64] **Branchiostegal ossifications.**

0 plate-like

1 narrow and ribbon-like

2 filamentous

65. [B:65] **Branchiostegal ossifications.**

0 ornamented

1 unornamented

66. [B:66] **Imbricated branchiostegal ossifications.**

0 absent

1 present

67. [B:67] **Median gular.**

0 absent

1 present

68. [B:68] **Lateral gular.**

0 absent

1 present

69. [B:69] **Opercular (submarginal) ossification.**

0 absent

1 present

70. [B:70] **Shape of opercular (submarginal) ossification.**

0 broad plate that tapers towards its proximal end

1 narrow, rod-shaped

71. [B:71] **Size of lateral gular plates.**

0 extending most of length of the lower jaw

1 restricted to the anterior third of the jaw (no longer than the width of three or four branchiostegals)

72. [B:72] **Gill arches.**

0 largely restricted to region under braincase

1 extend far posterior to braincase

73. [B:73] **Basihyal.**

0 absent

1 present

74. [B:74] **Interhyal.**

0 absent

1 present

75. [B:75] **Hypohyal.**

0 absent

1 present

76. [B:76] **Endoskeletal urohyal.**

0 absent

1 present

77. [B:77] **Oral dermal tubercles borne on jaw cartilages or at margins of the mouth.**

0 absent

1 present

78. [B:78] **Oral dermal tubercles patterned in organised rows (teeth).**

0 absent

1 present

79. [B:79] **Enamel(oid) on teeth.**

0 absent

1 present

80. [B:80] **Cap of enameloid restricted to upper part of teeth (acrodin).**

0 absent

1 present

81. [C:79] **Tooth families/whorls.**

0 absent

1 present

82. [B:82] **Bases of tooth whorls.**

0 single, continuous plate

1 some or all whorls consist of separate tooth units

83. [B:83] **Distribution of tooth whorls.**

0 entire length of tooth row

1 restricted to symphysial region

84. [B:84] **Distribution of tooth whorls.**

0 lower jaws only

1 upper and lower jaws

2 upper jaws only

85. [B:85] **Teeth ankylosed to dermal bones.**

0 absent

1 present

86. [B:86] **Plicidentine.**

0 absent

1 present

87. [B:87] **Dermal jaw plates on biting surface of jaw cartilages.**

0 absent

1 present

88. [B:88] **Maxillary and dentary marginal bones of mouth.**

0 absent

1 present

89. [B:89] **Premaxilla.**

0 extends under orbit

1 restricted anterior to orbit

90. [B:90] **Maxilla shape.**

0 splint-shaped

1 cleaver-shaped

91. [B:91] **Pair of tooth plates (anterior supragnathals or vomers) on ethmoidal plate.**

0 absent

1 present

92. [B:92] **Strong posterior flexion of dentary symphysis.**

0 absent

1 present

93. [B:93] **Extent of infradentaries.**

0 along much of ventral margin of dentary

1 restricted to posterior half of dentary

94. [B:94] **Coronoid fangs.**

0 absent

1 present

95. [B:95] **Position of upper mandibular arch cartilage (and associated cheek plate where present).**

0 entirely suborbital

1 with a postorbital extension

96. [B:96] **Position of mandibular arch articulations.**

0 terminal

1 subterminal

97. [B:97] **Autopalatine and quadrate.**

0 comineralized

1 separate mineralizations

98. [B:98] **Large otic process of the palatoquadrate.**

0 absent

1 present

99. [B:99] **Insertion area for jaw adductor muscles on palatoquadrate.**

0 ventral or medial

1 lateral

100. [B:100] **Palatoquadrate fused with neurocranium.**

0 absent

1 present

101. [B:101] **Oblique ridge or groove along medial face of palatoquadrate.**

0 absent

1 present

102. [B:102] **Fenestration of palatoquadrate at basipterygoid articulation.**

0 absent

1 present

103. [B:103] **Perforate or fenestrate anterodorsal (metapterygoid) portion of palatoquadrate.**

0 absent

1 present

104. [B:104] **Pronounced dorsal process on Meckelian bone or cartilage.**

0 absent

1 present

105. [B:105] **Number of coronoids.**

0 four or more

1 three or fewer

106. [B:106] **Preglenoid process.**

0 absent

1 present

107. [B:107] **Jaw articulation located on rearmost extremity of mandible.**

0 absent

1 present

108. [B:108] **Precerebral fontanelle.**

0 absent

1 present

109. [B:109] **Median dermal bone of palate (parasphenoid).**

0 absent

1 present

110. [B:110] **Parasphenoid.**

0 lozenge-shaped

1 splint-shaped

2 diamond-shaped

111. [B:111] **Multifid anterior margin of parasphenoid denticle plate.**

0 absent

1 present

112. [B:112] **Enlarged ascending processes of parasphenoid.**

0 absent

1 present

113. [B:113] **Buccohypophysial canal in parasphenoid.**

0 single

1 paired

114. [B:114] **Nasal opening(s).**

0 dorsal, placed between orbits

1 ventral and anterior to orbit

115. [B:115] **External opening of posterior nostril and orbit.**

0 separated by dermal bone(s)

1 confluent

116. [B:116] **Olfactory tracts.**

0 short, with olfactory capsules situated close to telencephalon cavity

1 elongate and tubular (much longer than wide)

117. [B:117] **Prominent pre-orbital rostral expansion of the neurocranium.**

0 present, formed of subethmoidal platform (‘upper lip’)

1 absent

2 present, formed of rhinocapsular block

118. [B:118] **Pronounced sub-ethmoidal keel.**

0 absent

1 present

119. [B:119] **Internasal vacuities.**

0 absent

1 present

120. [B:120] **Discrete division of the ethmoid and more posterior braincase at the level of the optic tract canal.**

0 absent

1 present

121. [B:121] **Position of myodome for superior oblique eye muscles.**

0 posterior and dorsal to foramen for nerve II

1 anterior and dorsal to foramen

122. [B:122] **Endoskeletal intracranial joint.**

0 absent

1 present

123. [B:123] **Spiracular groove on basicranial surface**

0 absent

1 present

124. [B:124] **Transverse otic process.**

0 present

1 absent

125. [B:125] **Jugular canal.**

0 long (invested in otic region along length of skeletal labyrinth)

1 short (restricted to short portion of region of skeletal labyrinth, or anterior to it)

2 absent (jugular vein uninvested in otic region)

126. [B:126] **Spiracular groove on lateral commissure.**

0 absent

1 present

127. [B:127] **Subpituitary fenestra.**

0 absent

1 present

128. [B:128] **Supraorbital shelf broad with convex lateral margin.**

0 absent

1 present

129. [B:129] **Orbit dorsal or facing dorsolaterally, surrounded laterally by endocranium.**

0 present

1 absent

130. [B:130] **Eyestalk attachment area.**

0 absent

1 present

131. [B:131] **Postorbital process.**

0 absent

1 present

132. [B:132] **Canal for jugular in postorbital process.**

0 absent

1 present

133. [B:133] **Series of perforations for innervation of supraorbital sensory canal in supraorbital shelf.**

0 absent

1 present

134. [B:134] **Extended prehypophysial portion of sphenoid.**

0 absent

1 present

135. [B:135] **Narrow interorbital septum, with outer walls in contact along midline forming a single sheet.**

0 absent

1 present

136. [B:136] **The main trunk of facial nerve (N. VII).**

0 elongate and passes anterolaterally through orbital floor

1 stout, divides within otic capsule at the level of the transverse otic wall

137. [B:137] **Course of hyoid ramus of facial nerve (N. VII) relative to jugular canal.**

0 traverses jugular canal, with separate exit in otic region

1 intersects jugular canal, with exit through posterior jugular foramen

138. [B:138] **Glossopharyngeal nerve (N. IX) exit.**

0 foramen situated posteroventral to otic capsule and anterior to metotic fissure

1 through metotic fissure

139. [B:139] **Relationship of cranial endocavity to basisphenoid.**

0 endocavity occupies full depth of sphenoid

1 enodcavity dorsally restricted

140. [B:140] **Subcranial ridges.**

0 absent

1 present

141. [B:141] **Ascending basisphenoid pillar pierced by common internal carotid.**

0 absent

1 present

142. [B:142] **Canal for lateral dorsal aorta within basicranial cartilage.**

0 absent

1 present

143. [B:143] **Entrance of internal carotids.**

0 through separate openings flanking the hypophyseal opening or recess

1 through a common opening at the central midline of the basicranium

144. [B:144] **Canal for efferent pseudobranchial artery within basicranial cartilage.**

0 absent

1 present

145. [B:145] **Position of basal/basipterygoid articulation.**

0 same anteroposterior level as hypophysial opening

1 anterior to hypophysial opening

2 posterior to hypophysial opening

146. [B:146] **Articulation between neurocanium and palatoquadrate posterodorsal to orbit (suprapterygoid articulation).**

0 absent

1 present

147. [B:147] **Labyrinth cavity.**

0 separated from the main neurocranial cavity by a cartilaginous or ossified capsular wall

1 skeletal capsular wall absent

148. [B:148] **Basipterygoid process (basal articulation) with vertically oriented component.**

0 absent

1 present

149. [B:149] **Pituitary vein canal.**

0 dorsal to level of basipterygoid process

1 flanked posteriorly by basipterygoid process

150. [B:150] **External (horizontal) semicircular canal.**

0 absent

1 present

151. [B:151] **Sinus superior.**

0 absent or indistinguishable from union of anterior and posterior canals with saccular chamber

1 present

152. [B:152] **External (horizontal) semicircular canal.**

0 joins the vestibular region dorsal to posterior ampulla

1 joins level with posterior ampulla

153. [B:153] **Horizontal semicircular canal in dorsal view.**

0 medial to path of jugular vein

1 dorsal to jugular vein

154. [B:154] **Lateral cranial canal.**

0 absent

1 present

155. [B:155] **Posterior dorsal fontanelle.**

0 absent

1 present

156. [B:156] **Shape of posterior dorsal fontanelle.**

0 approximately as long as broad

1 much longer than wide, slot-shaped

157. [B:157] **Synotic tectum.**

0 absent

1 present

158. [B:158] **Dorsal ridge.**

0 absent

1 present

159. [B:159] **Shape of median dorsal ridge anterior to endolymphatic fossa.**

0 developed as a squared-off ridge or otherwise ungrooved

1 bears a midline groove

160. [B:160] **Endolymphatic ducts in neurocranium.**

0 posteriodorsally angled tubes

1 tubes oriented vertically through median endolymphatic fossa

161. [B:161] **Position of hyomandibula articulation on neurocranium.**

0 below or anterior to orbit, on ventrolateral angle of braincase

1 on otic capsule, posterior to orbit

162. [B:162] **Position of hyomandibula articulation relative to structure of skeletal labyrinth.**

0 anterior or lateral to skeletal labyrinth

1 at level of posterior semicircular canal

163. [B:163] **Hyoid arch articulation on braincase.**

0 single

1 double

164. [B:164] **Branchial ridges.**

0 present

1 reduced to vagal process

2 absent (articulation made with bare cranial wall)

165. [B:165] **Craniospinal process.**

0 absent

1 present

166. [B:166] **Ventral cranial fissure.**

0 absent

1 present

167. [B:167] **Basicranial fenestra.**

0 absent

1 present

168. [B:168] **Metotic (otic-occipital) fissure.**

0 absent

1 present

169. [B:169] **Vestibular fontanelle.**

0 absent

1 present

170. [B:170] **Occipital arch wedged in between otic capsules.**

0 absent

1 present

171. [B:171] **Spino-occipital nerve foramina.**

0 two or more, aligned horizontally

1 one or two, dorsoventrally offset

172. [B:172] **Ventral notch between parachordals.**

0 present or entirely unfused

1 absent

173. [B:173] **Parachordal shape.**

0 forming a broad, flat surface as wide as the otic capsules

1 mediolaterally constricted relative to the otic capsules

174. [B:174] **Stalk-shaped parachordal/occipital region.**

0 absent

1 present

175. [B:175] **Paired occipital facets.**

0 absent

1 present

176. [B:176] **Size of aperture to notochordal canal.**

0 much smaller than foramen magnum

1 as large, or larger, than foramen magnum

177. [B:177] **Canal for median dorsal aorta within basicranium.**

0 absent

1 present

178. [B:178] **Hypotic lamina (and dorsally directed glossopharyngeal canal).**

0 absent

1 present

179. [B:179] **Macromeric dermal shoulder girdle.**

0 present

1 absent

180. [B:180] **Dermal shoulder girdle composition.**

0 ventral and dorsal (scapular) components

1 ventral components only

181. [B:181] **Shape of dorsal blade of dermal shoulder girdle (either cleithrum or anterolateral plate).**

0 spatulate

1 pointed

182. [B:182] **Dermal shoulder girdle forming a complete ring around the trunk.**

0 present

1 absent

183. [B:183] **Pectoral fenestra completely encircled by dermal shoulder armour.**

0 present

1 absent

184. [B:184] **Median dorsal plate.**

0 absent

1 present

185. [B:185] **Posterior dorsolateral (PDL) plate or equivalent.**

0 absent

1 present

186. [B:186] **Pronounced internal median keel on dorsal shoulder girdle (i.e., crista of median dorsal plate).**

0 absent

1 present

187. [B:187] **Crista internalis of dermal shoulder girdle.**

0 absent

1 present

188. [B:188] **Scapular infundibulum.**

0 absent

1 present

189. [B:189] **Scapular process of shoulder endoskeleton.**

0 absent

1 present

190. [B:190] **Ventral margin of separate scapular ossification.**

0 horizontal

1 deeply angled

191. [B:191] **Cross sectional shape of scapular process.**

0 flattened or strongly ovate

1 subcircular

192. [B:192] **Flange on trailing edge of scapulocoracoid.**

0 absent

1 present

193. [B:193] **Scapular process with posterodorsal angle.**

0 absent

1 present

194. [B:194] **Endoskeletal postbranchial lamina on scapular process.**

0 present

1 absent

195. [B:195] **Mineralisation of internal surface of scapular blade.**

0 mineralised all around

1 unmineralised on internal face forming a hemicylindrical cross-section

196. [B:196] **Coracoid process.**

0 absent

1 present

197. [B:197] **Procoracoid mineralisation.**

0 absent

1 present

198. [B:198] **Fin base articulation on scapulocoracoid.**

0 deeper than wide (stenobasal)

1 wider than deep (eurybasal)

199. [B:199] **Pectoral fin articulation.**

0 monobasal

1 polybasal

200. [B:200] **Number of basals in polybasal pectoral fins.**

0 three or more

1 two

201. [B:201] **Branching radials in paired fins.**

0 absent

1 present

202. [B:202] **Number of mesomeres in metapterygial axis.**

0 five or fewer

1 seven or more

203. [B:203] **Biserial pectoral fin endoskeleton.**

0 absent

1 present

204. [B:204] **Perforate propterygium.**

0 absent

1 present

205. [B:205] **Filamentous extension of pectoral fin from axillary region.**

0 absent

1 present

206. [B:206] **Pelvic fins.**

0 absent

1 present

207. [B:207] **Pelvic claspers.**

0 absent

1 present

208. [B:208] **Dermal pelvic clasper ossifications.**

0 absent

1 present

209. [B:209] **Pectoral fins covered in macromeric dermal armour.**

0 absent

1 present

210. [B:210] **Pectoral fin base has large, hemispherical dermal component.**

0 absent

1 present

211. [B:211] **Dorsal fin spines.**

0 absent

1 present

212. [B:212] **Anal fin spine.**

0 absent

1 present

213. [B:213] **Paired fin spines.**

0 absent

1 present

214. [B:214] **Median fin spine insertion.**

0 shallow, not greatly deeper than dermal bones/scales

1 deep

215. [B:215] **Prepelvic fin spines (modified).**

We follow Burrow et al.[21] and Hanke & Wilson[22] in labelling the fin spine pairs developed between the pectoral and pelvic fin spines as 'prepelvic' instead of the 'intermediate' used by Brazeau et al.[18]

0 absent

1 present

216. [B:216] **Fin spine cross-section.**

0 Round or horseshoe shaped

1 Flat-sided, with rectangular profile

217. [B:217] **Prepelvic spines when present (modified).**

See comments on character 215.

0 one pair

1 multiple pairs

218. [B:218] **Paired prepectoral spines (modified).**

Modified to enable coding for lateral pairs of prepectoral spines.

0 absent

1 present

219. [B:219] **Fin spines with ridges.**

0 absent

1 present

220. [B:220] **Fin spines with nodes.**

0 absent

1 present

221. [B:221] **Fin spines with rows of large retrorse denticles.**

0 absent

1 present

222. [B:222] **Expanded spine rib on leading edge of spine.**

0 absent

1 present

223. [B:223] **Spine ridges**

0 converging at the distal apex of the spine

1 converging on leading edge of spine

224. [B:224] **Synarcual.**

0 absent

1 present

225. [B:225] **Series of thoracic supraneurals.**

0 absent

1 present

226. [B:226] **Number of dorsal fins, if present.**

0 one

1 two

227. [B:227] **Posterior dorsal fin shape.**

0 base approximately as broad as tall, not broader than all of other median fins

1 base much longer than the height of the fin, substantially longer than any of the other dorsal fins

228. [B:228] **Basal plate in dorsal fin.**

0 absent

1 present

229. [B:229] **Branching radial structure articulating with dorsal fin basal plate.**

0 absent

1 present

230. [B:230] **Anal fin.**

0 absent

1 present

231. [B:231] **Basal plate in anal fin.**

0 absent

1 present

232. [B:232] **Caudal radials.**

0 extend beyond level of body wall and deep into hypochordal lobe

1 radials restricted to axial lobe

233. [B:233] **Supraneurals in axial lobe of caudal fin.**

0 absent

1 present

234. [B:234] **Epichordal lepidotrichia in caudal fin.**

0 absent

1 present

235. [B:235] **Enamel and pore canals.**

0 enamel absent from inner surface of pores

1 enamel lines portions of pore canal

236. [B:236] **Canal-bearing bone of skull roof extends far past posterior margin of parietals.**

0 no

1 yes

237. [B:237] **Pineal eminence (in taxa lacking pineal foramen).**

0 absent

1 present

238. [B:238] **Position of anterior pitline.**

0 on postparietal

1 on parietal

239. [B:239] **Opening in dermal skull roof for spiracular bounded by bones carrying otic canal.**

0 absent

1 present

240. [B:240] **Median skull roof bone between postparietals.**

0 absent

1 present

241. [B:241] **Westoll lines.**

0 absent

1 present

242. [B:242] **Preoperculosubmandibular.**

0 absent

1 present

243. [B:243] **Hyomandibula.**

0 imperforate

1 perforate

244. [B:244] **Urohyal shape.**

0 absent

1 vertical plate

245. [B:245] **Maxilla (in taxa with marginal jaw bones).**

0 present

1 absent

246. [B:246] **Length of dentary.**

0 constitutes a majority of jaw length

1 half the length of jaw or less

247. [B:247] **Labial pit.**

0 absent

1 present

248. [B:248] **Prearticular symphysis.**

0 absent

1 present

249. [B:249] **Mandibular sensory canal.**

0 extends through infradentaries

1 extends through infradentaries and dentary

250. [B:250] **Extensive flange composed of prearticular and Meckelian bone that extends beyond ventral edge of outer dermal series.**

0 absent

1 present

251. [B:251] **Posterior coronoid.**

0 similar to anterior coronoids

1 forms expanded coronoid process

252. [B:252] **Retroarticular process.**

0 absent

1 present

253. [B:253] **Inturned medial process of premaxilla.**

0 absent

1 present

254. [B:254] **Anteriorly directed adductor fossae between neurocranium and skull roof.**

0 absent

1 present

255. [B:255] **Vomerine fangs.**

0 absent

1 present

256. [B:256] **Number of dermopalatines.**

0 multiple

1 one

257. [B:257] **Entopterygoids.**

0 separated

1 contact along midline

258. [B:258] **Rostral tubuli.**

0 absent

1 present

259. [B:259] **Position of anterior nostril.**

0 facial

1 at oral margin

260. [B:260] **Posterior nostril.**

0 facial

1 at margin of oral cavity

2 palatal

261. [B:261] **Three large pores (in addition to nostrils) associated with each side of ethmoid.**

0 absent

1 present

262. [B:262] **Ventral face of nasal capsule in taxa with mineralized ethmoid.**

0 complete

1 fenestra ventrolateralis

2 entire floor unmineralized

263. [B:263] **Size of profundus canal in postnasal wall.**

0 small

1 large

264. [B:264] **Paired pineal and parapineal tracts.**

0 absent

1 present

265. [B:265] **Posterior of parasphenoid.**

0 restricted to ethmosphenoid region

1 extends to otic region

266. [B:266] **Endoskeletal spiracular canal.**

0 open

1 spiracular bar

2 complete enclosure in canal

267. [B:267] **Barbed lepidotrichial segments.**

0 absent

1 present

268. [B:268] **Relative position of jugular groove/canal and hyomandibular articulation.**

0 hyomandibula dorsal

1 hmd straddles

2 hmd ventral

269. [B:269] **Optic lobes.**

0 narrower than cerebellum

1 same width or wider than cerebellum

270. [B:270] **Hypophyseal chamber.**

0 projects posteroventrally

1 projects ventrally or anteroventrally

271. [B:271] **Crus commune of anterior and posterior semicircular canals.**

0 dorsal to braincase endocavity roof

1 ventral to braincase endocavity roof

272. [B:272] **Horizontal semicircular canal.**

0 obiquely oriented

1 horizontally oriented

273. [B:273] **Supraotic cavity.**

0 absent

1 present

274. [B:274] **Pelvic girdle with substantial dermal component.**

0 present

1 absent

275. [B:275] **Pelvic fin spines.**

0 absent

1 present

276. [B:276] **Pelvic fin.**

0 monobasal

1 polybasal

277. [B:277] **Postparietals/centrals.**

0 absent

1 present

278. [B:278] **Condition of postparietals/centrals.**

0 do not meet in midline

1 meet in midline

2 single midline bone

279. [B:279] **Parietals.**

0 absent

1 present

280. [B:280] **Condition of parietals.**

0 do not meet in midline

1 meet in midline

281. [B:281] **Endoskeletal lamina (postnasal wall) separating posterior nostril and orbit.**

0 absent

1 present

282. [B:282] **Pituitary vein canal.**

0 discontinuous, enters the cranial cavity

1 discontinuous, enters hypophysial recess

2 continuous transverse vein

283. [B:283] **Sutures between dermal bones.**

0 absent

1 present

284. [B:284] **Interolateral/clavicular margin.**

0 angled anterolaterally

1 mediolaterally straight

285. Scale odontodes added in a linear sequence within rows (linear odontocomplexes) (new character).

0 absent

1 present

286. Number of linear odontocomplexes in scale crowns (new character).

0 one

1 more than one

287. [D:262] **Anteriormost prepelvic fin spine (admedian fin spine) associated with the shoulder girdle (modified).**

We agree with Dearden et al.[17] in recognising the shoulder girdle spines positioned medially of the pectoral fin spines in a number of stem chondrichthyans (e.g. climatiids[8,9], diplacanthids[16] and gyracanthids[23]) as the first prepelvic fin spine pair. Here these are labelled admedian after Burrow et al.[7,8,16], who contrary to this and other studies[17,24] consider them separate from the prepelvic series.

0 absent

1 present

288. [K:482] **Median ventral prepectoral spine.**

0 absent

1 present

289. [K:447] **Median ventral trunk plates.**

0 absent

1 present

290. Direction of tooth addition within tooth families relative to the jaw ramus (new character).

0 lingual

1 mesial

2 distal

291. [B:17] **Odontode resorption in the extra-oral dermal skeleton (modified).**

See comments on character 17.

0 absent

1 present

292. Pinnal plates of the dermal shoulder girdle (new character).

Pinnal plates are distinguished from the dermal plates of jawed stem gnathostomes ('placoderms')[25,26] and osteichthyans[27-29] due to developmental differences. The latter form as a single unit through areal growth unlike the pinnals where independent dermal scales are integrated into discrete elements fused together by a basal plate[8,16,30] (see also this study). On this basis, and in accordance with previous research[31], we code for presence/absence of pinnal plates independently of the pectoral ventral plate pairs of 'placoderms' (ventrolateral plates) and osteichthyans (clavicles).

0 absent

1 present

Table S1. Relative abundance of *Fanjingshania* dermoskeletal elements estimated from a subsample (c. 500 specimens) of the material recovered from the Rongxi

Formation at Leijiatun (Extended Data Fig. 1). Relative abundance: X, very low; XX, low; XXX, medium; XXXX, high.

Element type	Relative abundance
trunk scales	XXXX
head tesserae	XXX
branchiostegal plates	X
pinnal plate fragments	XX
lorical plate fragments	X
prepectoral spines	X
pectoral fin spines	XX
prepelvic fin spines	XXX
pelvic fin spines	X
anterior dorsal fin spines	XX
posterior dorsal fin spines	XX
anal fin spines	XX

Table S2. Tip (taxon) ages for the time-scaled 50 percent majority-rule tree shown in part in Fig. 3 (full tree available in Supplementary data 7).

Taxon	Age in million years	Reference
Acanthodes	298	King et al.[20]
Achoania	412	King et al.[20]
Akmonistion	327	King et al.[20]
Austroptyctodus	327	King et al.[20]
Bothriolepis	383	King et al.[20]
Brachyacanthus	415	King et al.[20]
Brindabellaspis	401	King et al.[20]
Brochoadmones	415	King et al.[20]
Buchanosteus	408	King et al.[20]
Campbellodus	383	King et al.[20]
Cassidiceps	415	King et al.[20]

Cheiracanthus	388	King et al.[20]
Cheirolepis	388	King et al.[20]
Chondrenchelys	338	King et al.[20]
Cladodoides	375	King et al.[20]
Cladoselache	360	King et al.[20]
Climatius	415	King et al.[20]
Cobelodus	325	King et al.[20]
Coccosteus	388	King et al.[20]
Compagopiscis	383	King et al.[20]
Cowralepis	383	King et al.[20]
Culmacanthus	385	King et al.[20]
Debeerius	320	King et al.[20]
Diabolepis	412	King et al.[20]
Dialipina	401	King et al.[20]
Dicksonosteus	411	King et al.[20]
Diplacanthus	388	King et al.[20]
Diplocercides	383	Long and Trinajstic[32]
Diplodoselache	336	King et al.[20] and Dick[33]
Dipterus	388	Gross[34]
Doliodus	395	King et al.[20]
Entelognathus	424	King et al.[20]
Eurycaraspis	385	King et al.[20]
Eusthenopteron	380	King et al.[20]
Euthacanthus	415	King et al.[20]
Galeaspida	436	King et al.[20]
Gavinia	385	Long[35]
Gemuendina	408	King et al.[20]
Gladbachus	388	Coates et al.[19]
Gladiobranchus	415	King et al.[20]
Glyptolepis	388	King et al.[20]
Gogonasus	383	King et al.[20]

Guiyu	424	King et al.[20]
Gyracanthides	388	Warren et al.[23]
Fanjingshania	439	this study
Halimacanthodes	383	Burrow et al.[36]
Hamiltonichthys	302	King et al.[20]
Helodus	311	King et al.[20]
Homalacanthus	380	King et al.[20]
Howqualepis	385	King et al.[20]
Incisoscutum	383	King et al.[20]
Iniopera	307	Pradel et al.[37]
Ischnacanthus	415	King et al.[20]
Jagorina	375	King et al.[20]
Janusiscus	415	King et al.[20]
Kansasiella	303	King et al.[20]
Kathemacanthus	415	King et al.[20]
Kentuckia	347	King et al.[20]
Kosoraspis	419	Vaškaninová et al.[38]
Kujdanowiaspis	411	King et al.[20]
Latviacanthus	404	King et al.[20]
Lawrenciella	303	Poplin 1984
'Ligulalepis'	401	King et al.[20]
Lophosteus	423	Schultze and Märss[39]
Lunaspis	408	King et al.[20]
Lupopsyrus	415	King et al.[20]
Macropetalichthys	390	King et al.[20]
Meemannia	412	King et al.[20]
Mesacanthus	415	King et al.[20]
Miguashaia	380	King et al.[20]
Mimipiscis	383	King et al.[20]
Minjinia	411	Brazeau et al.[18]
Moythomasia	383	King et al.[20]

Nerepisacanthus	423	King et al.[20]
Obtusacanthus	415	King et al.[20]
Onychodus	383	King et al.[20]
Onychoselache	336	King et al.[20]
Orthacanthus	290	King et al.[20]
Osteostraci	427	King et al.[20]
Parayunnanolepis	412	King et al.[20]
Parexus	415	King et al.[20]
Poracanthodes	417	King et al.[20]
Porolepis	411	King et al.[20]
Powichthys	411	King et al.[20]
Promesacanthus	415	King et al.[20]
Psarolepis	416	King et al.[20]
Pterichthyodes	389	King et al.[20]
Ptomacanthus	415	King et al.[20]
Ptyctolepis	411	Lu et al.[40]
Pucapampella	388	King et al.[20]
Qingmenodus	411	Lu and Zhu[41]
Ramirosuarezia	392	King et al.[20]
Raynerius	373	Giles et al.[42]
Rhadinacanthus	388	Burrow et al.[16]
Rhamphodopsis	388	King et al.[20]
Romundina	415	King et al.[20]
Sparalepis	424	King et al.[20]
Styloichthys	412	King et al.[20]
Tamiobatis	360	King et al.[20]
Tetanopsyrus	415	King et al.[20]
Tristychius	336	King et al.[20]
Uranolophus	411	Denison[43]
Vernicomacanthus	415	King et al.[20]
Youngolepis	412	King et al.[20]

Yunnanolepis	415	King et al.[20]

Descriptions of supplementary files

Supplementary Data 1. A set of tomographic slices from a synchrotron X-ray radiation analysis of the holotype specimen of *Fanjingshania* (V27433.1). Tomographic slices generated in Mimics 19.0.

Supplementary Data 2. A set of tomographic slices from a synchrotron X-ray radiation analysis of *Fanjingshania* specimen V27434.1. Tomographic slices generated in Mimics 19.0.

Supplementary Data 3. A set of tomographic slices from a synchrotron X-ray radiation analysis of *Fanjingshania* specimen V27435.1. Tomographic slices generated in Mimics 19.0.

Supplementary Data 4. Volume rendering of *Fanjingshania* V27433.1 with colour coded features (see Fig. 2 for interpretation). 3D reconstruction and segmentation of synchrotron tomography data performed in Mimics 19.0.

Supplementary Data 5. Volume rendering of a *Fanjingshania* specimen V27434.1 with colour coded features (see Fig. 2 for interpretation). 3D reconstruction and segmentation of synchrotron tomography data performed in Mimics 19.0.

Supplementary Data 6. Volume rendering of the holotype of a *Fanjingshania* specimen V27435.1 with colour coded features (see Fig. 2 for interpretation). 3D reconstruction and segmentation of synchrotron tomography data performed in Mimics 19.0.

Supplementary Data 7. Parsimony analysis files. Character-taxon matrix in TNT (.tnt) and nexus (.nex) file formats**.** Most parsimonious trees (.tre) produced by the parsimony analysis. 50 percent majority-rule consensus tree (.tre) and strict consensus tree (.tre) for the set of most parsimonious trees. TNT log in rich text format (.rtf) of the parsimony and the bootstrap resampling analyses. PAUP log file (.log) of reconstructed character states at internal nodes of the 50 percent majority-rule consensus tree. R script in rich text format (.rtf) used in the calculation of the time-scaled 50 percent majority-rule consensus tree.

Supplementary Data 8. Bayesian analysis files. Character-taxon matrix (.nex), consensus tree (.tre) and other output files (.ckp, .mcmc, .parts, .t, tprobs, .tstat and .vstat) generated in MrBayes version 3.2.7a.

Supplementary references

1 Rong, J. *et al.* Silurian integrative stratigraphy and timescale of China. *Sci. China Earth Sci.* **62**, 89-111 (2018).

2 Wang, C.-Y. & Aldridge, R. J. Silurian conodonts from the Yangtze Platform, South China. *Spec. Pap. Palaeontol.* **83**, 1-135 (2010).

3 Zhou, X., Zhai, Z.-Q. & Xian, S. On the Silurian conodont biostratigraphy, new genera and species in Guizhou Province. *Oil Gas Geol.* **2**, 123-140 (1981).

4 Chen, Z. *et al.* Age of the Silurian Lower Red Beds in South China: Stratigraphical Evidence from the Sanbaiti Section. *J. Earth Sci.* **32**, 524-533 (2021).

5 Wang, C.-Y., Chen, L., Wang, Y. & Tang, P. Affirmation of *Pterospathodus eopennatus* Zone (Conodonta) and the age of the Silurian Shamao Formation in Zigui, Hubei as well as the correlation of the related strata. *Acta Palaeont. Sin.* **49**, 10-28 (2010).

6 Wang, C.-Y. Restudy on the ages of Silurian red beds in South China. *J. Stratigr.* **35**, 440-447 (2011).

7 Burrow, C. J., Newman, M. J., Davidson, R. G. & den Blaauwen, J. L. Redescription of *Parexus recurvus*, an Early Devonian acanthodian from the Midland Valley of Scotland. *Alcheringa* **37**, 392-414 (2013).

8 Burrow, C. J., Davidson, R. G., Den Blaauwen, J. L. & Newman, M. J. Revision of *Climatius reticulatus* Agassiz, 1844 (Acanthodii, Climatiidae), from the Lower Devonian of Scotland, based on new histological and morphological data. *J. Vertebr. Paleont.* **35**, e913421 (2015).

9 Miles, R. S. Articulated acanthodian fishes from the Old Red Sandstone of England: with a review of the structure and evolution of the acanthodian shoulder-girdle. *Bull. Br. Mus. Nat. Hist. Geol.* **24**, 111-213 (1973).

10 Miles, R. The acanthodian fishes of the Devonian Plattenkalk of the Paffrath Trough in the Rhineland. *Arkiv für Zoologi* **18**, 147-194 (1966).

11 Denison, R. *Acanthodii*. Vol. 5 (Gustav Fischer Verlag, 1979).

12 Dearden, R. P. *The Anatomy and Evolution of "Acanthodian" Stem-chondrichthyans* (Imperial College London, 2018).

13 Dearden, R. P. *et al.* A revision of *Vernicomacanthus* Miles with comments on the characters of stem-group chondrichthyans. *Pap. Palaeontol.* **7**, 1949-1976 (2021).

14 Watson, D. M. S. II-The Acanthodian fishes. *Philos. Trans. R. Soc. Lond. Ser. B, Biol. Sci.* **228**, 49-146 (1937).

15 Ørvig, T. Some new acanthodian material from the Lower Devonian of Europe. *Zool. J. Linn. Soc.* **47**, 131-153 (1967).

16 Burrow, C., den Blaauwen, J., Newman, M. & Davidson, R. The diplacanthid fishes (Acanthodii, Diplacanthiformes, Diplacanthidae) from the Middle Devonian of Scotland. *Palaeontol. Electron.* **19**, 1-83 (2016).

17 Dearden, R. P., Stockey, C. & Brazeau, M. D. The pharynx of the stem-chondrichthyan *Ptomacanthus* and the early evolution of the gnathostome gill skeleton. *Nat. Commun.* **10**, 2050 (2019).

18 Brazeau, M. *et al.* Endochondral bone in an Early Devonian'placoderm'from Mongolia. *Nat. Ecol. Evol.* **4**, 1477–1484 (2020).

19 Coates, M. I. *et al.* An early chondrichthyan and the evolutionary assembly of a shark body plan. *Proc. R. Soc B* **285**, 20172418 (2018).

20 King, B., Qiao, T., Lee, M. S., Zhu, M. & Long, J. A. Bayesian morphological clock methods resurrect placoderm monophyly and reveal rapid early evolution in jawed vertebrates. *Syst. Biol.* **66**, 499-516 (2017).
21 Brazeau, M. D. & Friedman, M. The origin and early phylogenetic history of jawed vertebrates. *Nature* **520**, 490-497 (2015).
22 Hanke, G. & Wilson, M. in *Morphology, Phylogeny and Paleobiogeography of Fossil Fishes*. 159-182 (Verlag Dr. Friedrich Pfeil, 2010).
23 Warren, A., Currie, B. P., Burrow, C. & Turner, S. A redescription and reinterpretation of *Gyracanthides murrayi* Woodward 1906 (Acanthodii, Gyracanthidae) from the Lower Carboniferous of the Mansfield Basin, Victoria, Australia. *J. Vertebr. Paleont.* **20**, 225-242 (2000).
24 Gagnier, P.-Y. & Wilson, M. V. Early Devonian acanthodians from northern Canada. *Palaeontology* **39**, 241-258 (1996).
25 Dupret, V., Sanchez, S., Goujet, D., Tafforeau, P. & Ahlberg, P. E. Bone vascularization and growth in placoderms (Vertebrata): The example of the premedian plate of *Romundina stellina* Ørvig, 1975. *C. R. Palevol* **9**, 369-375 (2010).
26 Giles, S., Rücklin, M. & Donoghue, P. C. Histology of "placoderm" dermal skeletons: Implications for the nature of the ancestral gnathostome. *J. Morphol.* **274**, 627-644 (2013).
27 Andrews, M., Long, J., Ahlberg, P., Barwick, R. & Campbell, K. The structure of the sarcopterygian *Onychodus jandemarrai* n. sp. from Gogo, Western Australia: with a functional interpretation of the skeleton. *Earth. Env. Sci. Trans. R. Soc. Edinb.* **96**, 197-307 (2005).
28 Mondéjar-Fernández, J., Friedman, M. & Giles, S. Redescription of the cranial skeleton of the Early Devonian (Emsian) sarcopterygian *Durialepis edentatus* Otto (Dipnomorpha, Porolepiformes). *Pap. Palaeontol.* (2020).
29 Zhu, M., Yu, X., Wang, W., Zhao, W. & Jia, L. A primitive fish provides key characters bearing on deep osteichthyan phylogeny. *Nature* **441**, 77-80 (2006).
30 Long, J. A new diplacanthoid acanthodian from the Late Devonian of Victoria. *Mem. Assoc. Australas. Palaeontol.* **1**, 51-65 (1983).
31 Moy-Thomas, J. & Miles, R. S. *Palaeozoic Fishes* (Chapman and Hall, 1971).
32 Long, J. A. & Trinajstic, K. The Late Devonian Gogo Formation lägerstatte of Western Australia: exceptional early vertebrate preservation and diversity. *Annu. Rev. Earth Planet Sci.* **38**, 255-279 (2010).
33 Dick, J. R. *Diplodoselache woodi* gen. et sp. nov., an early Carboniferous shark from the Midland Valley of Scotland. *Earth Environ. Sci. Trans. R. Soc. Edinb.* **72**, 99-113 (1981).
34 Gross, W. Über die Randzähne des Mundes, die Ethmoidalregion des Schädels und die Unterkiefersymphyse von *Dipterus oervigi* n. sp. *Paläontol. Z.* **38**, 7-25 (1964).
35 Long, J. A. A new genus of fossil coelacanth (Osteichthyes: Coelacanthiformes) from the Middle Devonian of southeastern Australia. *Rec. West. Aust. Mus., Suppl.* **57**, 37-53 (1999).
36 Burrow, C. J., Trinajstic, K. & Long, J. First acanthodian from the Upper Devonian (Frasnian) Gogo Formation, Western Australia. *Hist. Biol.* **24**, 349-357 (2012).
37 Pradel, A., Tafforeau, P. & Janvier, P. Study of the pectoral girdle and fins of the Late Carboniferous sibyrhynchid iniopterygians (Vertebrata, Chondrichthyes, Iniopterygia) from Kansas and Oklahoma (USA) by means of microtomography, with comments on iniopterygian relationships. *C. R. Palevol* **9**, 377-387 (2010).
38 Vaškaninová, V. *et al.* Marginal dentition and multiple dermal jawbones as the ancestral condition of jawed vertebrates. *Science* **369**, 211-216 (2020).
39 Schultze, H.-P. & Märss, T. Revisiting *Lophosteus*, a primitive osteichthyan. *Acta Univ. Latv.* **679**, 57-78 (2004).
40 Lu, J., Giles, S., Friedman, M. & Zhu, M. A new stem sarcopterygian illuminates patterns of character evolution in early bony fishes. *Nat. Commun.* **8**, 1932 (2017).

41 Lu, J. & Zhu, M. An onychodont fish (Osteichthyes, Sarcopterygii) from the Early Devonian of China, and the evolution of the Onychodontiformes. *Proc. R. Soc. B: Biol. Sci.* **277**, 293-299 (2010).
42 Giles, S., Friedman, M. & Brazeau, M. D. Osteichthyan-like cranial conditions in an Early Devonian stem gnathostome. *Nature* **520**, 82-85 (2015).
43 Denison, R. H. Early Devonian lungfishes from Wyoming, Utah, and Idaho. *Field Mus. Nat. Hist. Bull.* **17**, 353–413 (1968).